Increased lactate secretion by cancer cells sustains non-cell-autonomous adaptive resistance to MET and EGFR targeted therapies

Maria Apicella[1], Elisa Giannoni[2], Stephany Fiore[1,3‡], Karin Johanna Ferrari[4], Fernández-Pérez Daniel[4,] Claudio Isella[1], Carlotta Granchi[5], Filippo Minutolo[5], Antonino Sottile[1], Paolo M. Comoglio[1], Enzo Medico[1,3], Filippo Pietrantonio[6], Marco Volante[3,7], Diego Pasini[4,8], Paola Chiarugi[2,9], Silvia Giordano[1,3,*§], Simona Corso[1,3,*§].

[1]Candiolo Cancer Institute - FPO, IRCCS, Candiolo, Italy ; [2]Dept. of Experimental and Clinical Biomedical Sciences, University of Florence, Florence, Italy; [3]University of Torino, Dept. Of Oncology, Candiolo, Italy; [4]Dept. of Experimental Oncology, European Institute of Oncology, Milan, Italy; [5]Dept. of Pharmacy, University of Pisa, Pisa, Italy; [6]Medical Oncology Department, Fondazione IRCCS Istituto Nazionale dei Tumori, Milan, Italy; [7]Pathology Unit, San Luigi Hospital, Orbassano, Italy; [8]Department of Health Sciences, University of Milan, Milan, Italy; [9]Tuscany Tumor Institute and "Center for Research, Transfer and High Education DenoTHE", Florence, Italy.

‡Current Affiliation: Dependence Receptors, Cancer and Development Laboratory, Centre de RechercheenCancérologie de Lyon, Inserm U1052-CNRS UMR5286, Université de Lyon, Centre Léon Bérard, Lyon, France.

Running Title: Lactate mediates adaptive resistance to TKIs

* **Correspondence:**

Simona Corso or Silvia Giordano (Lead contact: Simona Corso)

IRCC, strada Provinciale 142, Candiolo, 10060 (Torino), Italy.

Phone: +39 011 9933233Fax: +39 011 9933225

Emails: simona.corso@unito.it;silvia.giordano@unito.it.

§ These two Authors equally contributed to the work.

Summary

Microenvironment is known to influence cancer drug response and sustain resistance to therapies targeting receptor-tyrosine kinases. However if and how tumor microenvironment can be altered during treatment, contributing to resistance onset is not known. Here we show that, under prolonged treatment with tyrosine kinase inhibitors (TKIs), EGFR- or MET-addicted cancer cells displayed a metabolic shift towards increased glycolysis and lactate production. We identified secreted lactate as the key molecule able to instruct Cancer Associated Fibroblasts (CAFs) to produce Hepatocyte Growth Factor (HGF) in a NF-KB dependent manner. Increased HGF, activating MET-dependent signaling in cancer cells, sustained resistance to TKIs. Functional or pharmacological targeting of molecules involved in the lactate axis, such as lactate dehydrogenase or the lactate transporters MCT4 and MCT1 abrogated *in vivo* resistance, demonstrating the crucial role of this metabolite in the adaptive process.

This non-cell-autonomous, adaptive resistance mechanism was observed in NSCLC patients progressed on EGFR TKIs, demonstrating the clinical relevance of our findings and opening novel scenarios in the challenge to drug resistance.

Keywords: HGF/MET, EGFR, targeted therapy, resistance, lactate, LDH, tumor metabolism, CAFs, tumor microenvironment.

Highlights:

- Lactate production is increased in MET/EGFR TKI-resistant cancer cells
- CAF lactate uptake stimulates HGF overexpression by NF-kB, driving adaptive resistance
- LDH, MCT4 and MCT1 inhibition abrogates *in vivo* adaptive resistance to MET/EGFR TKIs
- Stromal HGF and tumor cell MCT4 were increased in EGFR-TKI resistant patients

eTOC Blurb

The metabolic interplay between tumor cells and CAFs drives adaptive resistance to MET and EGFR targeted therapies. To our knowledge, this is the first report identifying a metabolism-driven, non-cell-autonomous mechanism of acquired resistance to TKIs, opening exciting clinical opportunities to bypass a major hurdle in cancer treatment.

INTRODUCTION

The clinical efficacy of anti-cancer targeted therapies is strongly limited by the rapid and inexorable development of acquired drug resistance. Therefore, understanding resistance-causing mechanisms is a critical challenge to improve the outcome of candidates for such treatment strategies. In the last decade, the use of *in vitro* models allowed the identification of a number of molecular mechanisms responsible for acquired resistance to tyrosine kinase inhibitors (TKIs). The clinical importance of these resistance models is unquestionable, as many *in vitro*-identified mechanisms of resistance have been subsequently translated in the clinic (Camidge et al., 2014; Engelman and Settleman, 2008; Lovly and Shaw, 2014). However, lacking the epithelial-stromal interactions typically occurring *in vivo, in vitro* models preclude the identification of possible non-cell-autonomous mechanisms of resistance. It is now firmly established that tumor microenvironment may affect important tumor functions, such as proliferation and metastatic ability, and can also influence treatment responses (Bhowmick et al., 2004; Shiao et al., 2011). Indeed, recent reports suggest an important role of tumor stroma in sustaining drug resistance, mediated by pro-inflammatory pathways or by the secretion of growth factors, able to activate in cancer cells transduction pathways compensatory to those pharmacologically inhibited (Carbone et al., 2011; Meads et al., 2009; Straussman et al., 2012; Wilson et al., 2012). In this context, a key role is played by the Hepatocyte Growth Factor (HGF), whose secretion by mesenchymal cells elicits activation of the MET tyrosine kinase receptor (Bottaro et al., 1991; Giordano et al., 1989). Several studies have shown that MET activation can broadly behave as a bypass mechanism, compensating for loss of drug-inhibited signaling pathways in several tumor contexts (Harbinski et al., 2012; Straussman et al., 2012; Wilson et al., 2012). However, whether and how cancer cells can instruct their microenvironment to activate resistance-mediating pathways is poorly known.

In order to identify and study non-cell-autonomous mechanisms of acquired resistance to molecular therapies, we generated *in vivo* models of acquired resistance to MET or EGFR (Epidermal Growth Factor Receptor) TKIs. MET has been extensively studied as a target for therapeutic intervention (Comoglio et al., 2008; Peters and Adjei, 2012) and evidence accumulated in the last decade suggests that, in selected contexts, MET targeting drugs displayed clinical efficacy in patients with tumors harboring *MET* oncogenic alterations(Cui, 2014; Gherardi et al., 2012). EGFR is an established therapeutic target in oncology. EGFR TKIs are the standard first line therapy for patients with *EGFR*-mutation positive advanced non-small cell lung cancer (NSCLC) (Maemondo et al., 2010; Mok et al., 2009; Rosell et al., 2012; Zhou et al., 2011) and are also approved for pancreatic cancer (Moore et al., 2007). Unfortunately, as usually reported for molecular therapies, patients initially responsive to MET or EGFR inhibitors invariably become resistant and progress (Camidge et al., 2014; Lennerz et al., 2011; Sequist et al., 2011; Yu et al., 2013).Even if preclinical studies led to the identification of several cell-autonomous mechanisms of acquired resistance(Cepero et al., 2010; Chong and Jänne, 2013; Corso et al., 2010; Dillon et al., 2011; Ohashi et al., 2013; Qi et al., 2011), we are far from having a comprehensive view of resistance causes. Indeed, for example, in about one third of NSCLCs, resistance to EGFR TKIs remains unexplained. In particular, non-cell-autonomous mechanisms have not been very adequately explored in preclinical studies and in the clinics.

The *in vivo* models of adaptive resistance to MET or EGFR TKIs we generated demonstrate that non-cell-autonomous factors can play a pivotal role in resistance onset. Notably we identified, for the first time, a metabolism-based mechanism of adaptive resistance, whereas TKI-induced metabolic switch of tumor cells, with increased lactate production, instructs CAFs to overproduce HGF, eventually enforcing drug resistance and tumor progression. Increased production of tumor lactate and stromal HGF, which are potentially targetable adaptive alterations, were detected in advanced

NSCLC patients upon emergence of resistance to EGFR TKIs, thus confirming the clinical relevance of our findings.

RESULTS

***In vivo*-generated tumor adaptive resistance to the MET TKI JNJ-605 is mediated by non-cell-autonomous mechanisms.**

To investigate *in vivo* mechanisms of acquired resistance to MET targeted therapies, we continuously treated mice bearing EBC1 (a MET-addicted NSCLC cell line(Cepero et al., 2010)) xenograft tumors with a specific anti-MET compound (JNJ-605)(Cepero et al., 2010), until resistance onset (RES-J tumors, Figure 1A; see Star Methods for details). Tumors grown in untreated animals represented matched controls (WT tumors). From each resistant and control tumor we derived cancer cell lines *ex vivo*. After few passages in culture, thanks to their faster growth rate, EBC1 tumor cells overwhelmed the fibroblasts present in the dish; this allowed obtaining a homogeneous cancer cell population (Figure S1A). Surprisingly, we observed that 4 out of 5 EBC1 cell lines derived from JNJ-605 resistant tumors (RES-J EBC1) were not resistant to the MET TKI *in vitro*, showing an IC_{50} similar to control cells (Figure 1B). Molecular analysis ruled out the presence of the most frequent genetic alterations known to confer resistance to MET TKIs (data not shown). However, when subcutaneously re-injected in mice, RES-J EBC1 cells re-originated drug-resistant tumors; as expected, re-injected WT EBC1 cells gave rise to drug-sensitive tumors (Figure 1C). This result suggests that RES-J EBC1, although not autonomously drug-resistant, had acquired the permanent ability to generate a drug-resistant tumor mass. In order to unravel the role of tumor microenvironment in the adaptive resistance to the MET TKI, we performed *in vivo* co-culture experiments. Luciferase-transduced parental EBC1 cells (EBC1 Luc), sensitive to MET TKIs, were injected in preformed WT or RES-J tumors, and mice were randomized into three experimental groups: (i) WT untreated tumors, (ii) WT tumors treated with JNJ-605 and (iii) RES-J tumors treated with JNJ-605. After six weeks of treatment, the animals were sacrificed and the level of the luciferase signal (proportional to the number of living EBC1 Luc cells) was evaluated by IVIS Imaging.

Interestingly, EBC1 Luc cells were not growth-inhibited by the MET TKI when injected inside pre-formed drug-resistant tumors, while they responded to drug treatment when injected into drug-sensitive (WT) tumors (Figure 1D). To identify the cellular component of RES-J tumors critical for conferring resistance to parental cancer cells, we first evaluated the role of RES-J EBC1 cells. EBC1 Luc cells were co-cultured *in vitro* with tumor-derived RES-J EBC1 cells or WT EBC1 cells, in the presence of increasing doses of JNJ-605. As shown, neither RES-J EBC1 cells nor WT EBC1 cells affected EBC1 Luc sensitivity to the MET inhibitor (Figure S1B), reinforcing the hypothesis that stromal populations could be responsible for the conferred resistance.

Cancer associated fibroblasts (CAFs) are the principal component of the tumor stroma and regulate tumor cell functions by secreting growth factors, chemokines, and extracellular matrix (Zhang and Liu, 2013). Several studies have previously reported tumor-stroma interactions capable of mediating chemo-resistance (Hu et al., 2015). Moreover, recent findings demonstrate that CAF-secreted factors can modulate responsiveness to targeted agents, in different tumor contexts (Straussman et al., 2012). We obtained pure mouse fibroblasts cultures from resistant or control tumors (RES-J CAF or WT CAF) (Figure S1A), by treating the collagenase-dissociated tumors with the diphtheria toxin, which selectively kills human (EBC1) but not mouse (stroma) cells (Arbiser et al., 1999). When tested in *in vitro* co-culture assays, CAFs derived from resistant tumors rendered WT EBC1 cells resistant to the MET TKI, even at high drug concentrations, while CAFs derived from control tumors induced resistance to low TKI doses only (Figure 1E). These results suggest that, in this model, the adaptive resistance to MET TKI treatment is not intrinsic to cancer cells, but it is due to the interplay with tumor stroma, in particular with CAFs.

Increased HGF production by CAFs is responsible for adaptive resistance to JNJ-605.

To understand if CAFs fuel resistance to JNJ-605 through secretion of soluble molecule(s), we treated EBC1 cells with increasing concentrations of JNJ-605, in presence or absence of RES-J or WT CAF conditioned media. Media obtained from different RES-J CAF populations strongly impaired EBC1 sensitivity to JNJ-605, while WT CAF media did not alter drug response (Figure 2A). This entails that the adaptive resistance to MET inhibitors was mediated by soluble factor(s) secreted by resistant CAFs. Interestingly, western blot analysis revealed that the presence of RES-J CAF conditioned media (but not of WTCAFs conditioned media) preserved MET phosphorylation and activation of MET downstream pathways in tumor cells, despite treatment with the MET TKI (Figure 2B). As it was previously shown that HGF, the MET ligand, causes a dose-dependent increase in the IC_{50} of MET TKIs, stabilizing MET homodimers (less sensitive to MET TKIs) and activating TKI-free receptors (Pennacchietti et al., 2014), we considered HGF involvement in resistance onset. Indeed, quantitative real time PCR and ELISA experiments revealed that *in vitro* RES-J CAFs expressed and secreted HGF at significantly higher levels compared to WT-CAFs (Figure 2C-D). An important stromal HGF mRNA increase was also confirmed *in vivo* through RNA *in situ* hybridization on formalin-fixed and paraffin embedded (FFPE) slides of the original resistant tumors, as well as on slides of resistant tumors generated upon RES-J EBC1 re-injection in mice (Figure 2E).

To prove that HGF was critical to mediate CAF-induced resistance, the conditioned medium of RES-J CAFs was depleted from HGF through heparin-binding; as shown in Figure2F, upon depletion, RES-J CAF-conditioned medium lost the ability to induce resistance, while re-introduction of purified murine HGF, at the concentration range found in the RES-J CAF medium, restored resistance to JNJ-605. These results demonstrate the causative role of CAF-produced HGF in this model of resistance. Notably, while mouse HGF was reported to activate only some of the MET-driven biological activities in human cells (Cecchi et al., 2015), we clearly observed that, in the specific context of resistance to

MET TKIs, mouse and human purified HGF exerted superimposable effects on human MET-addicted cells, inducing a similar shift of the TKI IC_{50} (Figure 2G).

Lactate is the key metabolite driving HGF upregulation in CAFs.

We demonstrated that increased production of stromal HGF is responsible for the tumor adaptive resistance to the MET TKI. Moreover, as shown in FIGURE1C and 2E, RES-J EBC1 cells, upon *in vivo* re-injection, were able to recreate a resistant tumor mass displaying stromal HGF overexpression. Trying to reproduce this phenomenon *in vitro,* we co-cultured WT CAFs with WT or RES-J EBC1 cells, in the presence of the MET inhibitor, and monitored mouse HGF production. Interestingly, after 3 weeks of co-culture with RES-J EBC1 cells (but not with WT EBC1), WT CAFs significantly increased their HGF production (Figure 3A). This demonstrates that RES-J EBC1 cells were directly able to instruct fibroblasts to overproduce MET ligand.

Next, we wondered which molecular mechanism enables RES-J EBC1 cells to instruct the microenvironment, promoting HGF expression in CAFs. It is known that tumor cells and CAFs are 'metabolically coupled' in a symbiotic relationship (Fiaschi et al., 2012; Salem et al., 2012). Moreover, resistant cells often present a marked Warburg metabolism which leads to production and secretion of high amounts of lactate (Bacci et al., 2016; Curtarello et al., 2015; Lai et al., 2014; Zhou et al., 2010). We thus wondered if RES-J EBC1 cells were metabolically different from their WT counterpart. An enzymatic assay performed on the supernatant of two different WT and RES-J EBC1 and of parental EBC1 cells revealed a significant increase in lactate release in RES-J cells compared to controls (Figure 3B); in parallel, analysis of [U-14C] glucose uptake showed a significant increase in glucose consumption in RES-J EBC1 cells, suggesting a higher exploitation of the glycolytic metabolism compared to control cells (Figure 3C). Moreover, increased expression of acknowledged markers of Warburg metabolism (hexokinase 2 [HK2], Glucose Transporter 1 [GLUT1],

Monocarboxylate transporter 4 [MCT4]) confirmed the metabolic switch of RES-J EBC1 towards aerobic glycolysis (FigureS1C).

We hypothesized that the metabolic reprogramming of resistant cells could promote HGF transcription in CAFs; indeed, HGF is a molecule often produced in response to extracellular stimuli that can modify cellular homeostasis (Carrolo et al., 2003; Pennacchietti et al., 2003; Zeng et al., 2002). Interestingly, exposure to lactate induced HGF transcriptional up-regulation in WT CAFs (Figure 3D), suggesting a key role of this metabolite in the observed adaptive resistance. Lactate release can induce media acidification; however, we proved that medium acidification did not cause any significant increase of HGF production in CAFs (data nor shown), ruling out the role of pH in the acquisition of resistance.

The metabolic switch observed in tumor cells could be reproduced *in vitro* by prolonged treatment of parental EBC1 cells with MET TKIs, but not by treatment with TKIs targeting kinases other than MET. Indeed EBC1 cells, cultured for 3 weeks in the presence of suboptimal doses of JNJ-605 or crizotinib (a multikinase MET inhibitor) increased their lactate release up to the levels observed in RES-J EBC1. No significant lactate increase was observed in EBC1 cells treated with TKIs targeting other kinases, such as erlotinib or TP-0903 (EGFR and AXL inhibitors, respectively) (Figure 3E). To understand if the metabolic switch was due to the selection of a preexisting high-Warburg population or to the metabolic adaptation of tumor cells, we measured glucose uptake in parental EBC1 cells using a fluorescent glucose analog (2-NBDG). Flow-cytometry analysis revealed a single 2-NBDG incorporation pick (Figure S21D, left panel). Moreover, when the two curve tails (corresponding to the most and least glycolytic cells) were sorted, cultured for 1 week and analysed for glucose uptake, they showed the same uptake profile of parental cells (Figure S1D, right panels). These results suggest that the metabolic switch observed in resistant EBC1 cells is not the result of the selection of a preexisting subpopulation displaying a higher Warburg metabolism.

Like RES-J EBC1, also RES-J CAFs showed an increased lactate release (Figure 3E) and glucose uptake (Figure 3F) compared to WT-CAFs, suggesting that CAFs themselves had undergone a metabolic switch. RNAseq data confirmed that RES-J CAFs showed features of enhanced glycolytic metabolism. Glucose and lactate transporters (MCT4, GLUT3), several glycolytic enzymes (PGM, PFK and ENO) and TCA inhibitors (PDKs) were indeed overexpressed in RES CAFs (Figure 3G) compared to WT CAFs. HGF overexpression in RES-J CAFs was indefinitely maintained in culture in the absence of RES-J EBC1 cells. However, pharmacologic or genetic inhibition in RES-J CAFs of either Lactate dehydrogenase (LDH) or the lactate importer MCT1 significantly decreased HGF mRNA levels in these cells (FigureS1E-G). These results suggest a crucial role of the glycolytic switch in CAFs for their indefinite HGF overexpression in culture.

To understand if the constitutive HGF overexpression in RES-J CAFs relies on epigenetic changes at the Hgf locus, we performed Chromatin immune-precipitation (ChIP) experiments. As shown in Figure S2A, marks of active transcription were differentially accumulated at the transcription start site (TSS) of the Hgf gene in RES-J CAFs compared to WT CAFs. Moreover, the H3K36me3, a modification linked to gene transcriptional elongation, resulted notably increased within the Hgf gene body, whereas repressive marks were not detectable at Hgf promoter in both CAF cells lines.

Lactate-induced HGF transcriptional upregulation in CAFs is mediated by NF-kB.

It is known that the NF-kB transcription factor can promote HGF gene transcription (Harrison and Farzaneh, 2000; Yin et al., 2014). Since it was previously reported that lactate stimulates the NF-kB pathway by triggering IkB α degradation (Végran et al., 2011), we explored if lactate-induced HGF overexpression in RES-J CAFs was mediated by this transcription factor. Indeed, western blot analysis showed a decrease of IkB α, as well as an increase of NF-kB levels in RES-J CAFs compared to WT CAFs (Figure 4A, left panel). Exposure to lactate concentrations in the range of those released

by RES-J CAFs induced in WT CAFs a reduction of IkBα levels and a concomitant increase in NF-kB expression, similar to that observed in RES-J CAFs (Figure 4A, left panel); this demonstrates that exposure to lactate is sufficient to induce CAF NF-kB upregulation. Importantly, we showed that NF-kB is required for HGF overexpression since CAF treatment with two different NF-kB pathway inhibitors (IKK-16 and BMS-345541), significantly reduced both lactate-induced HGF upregulation in WT CAFs and basal HGF overexpression in RES-J CAF (Figure 4B and Figure 4A, central and right panels). Importantly, the conditioned medium of RES-J CAFs grown in the presence of NF-kB pathway inhibitors lost the ability to confer resistance to JNJ-605 (Figure 4C), as it contained HGF levels similar to WT CAF medium (FigureS2C). These data prove the requirement of NF-kB activity in the lactate-HGF axis.

Pharmacologic inhibition and genetic interference of lactate metabolism bypass adaptive resistance to MET inhibition in different MET-addicted models.

Since the adaptive resistance to MET TKIs in EBC1 tumors was strongly linked to a metabolic tumor rewiring and, in particular, to increased lactate production and efflux from tumor cells, and influx in CAFs, we explored the possible therapeutic potential of these findings.

We subcutaneously re-injected RES-J EBC1 cells in mice that were treated with either vehicle or the LDH inhibitor NHI-Glc-2 (Calvaresi et al., 2013), in the absence or presence of JNJ-605. While NHI-Glc-2 treatment (50 mg/kg) significantly decreased the NAD+/NADH ratio inside the tumors, (Figure S3B), it did not impair tumor growth but it completely prevented the onset of resistance to JNJ-605 (Figure 5A). The combo treatment was well tolerated by mice which did not show significant alterations in hepatic or renal function (Figure S3A). Similar results were obtained through genetic LDH inhibition in tumor cells as well. RES-J EBC1 cells were stably interfered with lentiviral vector particles encoding for 2 different couples of short hairpin RNAs targeting the two LDH isoforms

expressed in these tumors, LDH A and B (shLDHA/B, FigureS3C), or for a control short hairpin RNA (shCRTL). When transduced cells were re-injected in mice, LDH silencing completely restored the response to JNJ-605. As for NHI-Glc-2 treatment, LDH silencing *per se* did not affect tumor growth (Figure 5B). Moreover, we demonstrated that pharmacologic LDH inhibition was able not only to prevent resistance onset, but also to overcome established resistance, as NHI-Glc-2 induced regression of already resistant tumors, re-sensitizing tumor cells to MET TKIs (Figure 5C).

Since lactate production in tumor cells was required to establish resistance, we then explored the effect of blocking lactate export from tumor cells into the microenvironment. We performed *in vivo* experiments by injecting mice with RES-J EBC1 cells stably transduced with two different MCT4 shRNAs (Figure S3D). As shown in Figure 5D, MCT4 abrogation in resistant tumor cells completely restored the response to MET TKIs. Moreover, as *in vitro* MCT1 inhibition in CAF was sufficient to revert their HGF overexpression (Figures S1 E-G), we also explored the effect of blocking lactate cell import during the *in vivo* establishment of resistance. Mice injected with RES-J EBC1 cells were treated with the AZD3965 MCT1 inhibitor (already in clinical investigation in humans, NCT01791595). As shown in Figure 5E, MCT1 inhibition significantly restored cancer cell sensitivity to TKIs.

Overall, these results demonstrate a crucial role of lactate metabolism in the adaptive resistance to MET TKI, and suggest LDH, MCT4 and MCT1 as possible therapeutic targets. Moreover, since in the silencing experiments LDH and MCT4 inhibition was restricted to the cancer cells, this formally demonstrates that lactate over-production and over-secretion by tumor cells can be considered the *primum movens* for the development of resistance.

This metabolism-driven, non-cell-autonomous mechanism of adaptive resistance to MET inhibition is not unique to the EBC1 model. In fact, also in the case of another MET-addicted cell line, GTL16

(derived from a gastric cancer (Smolen et al., 2006)), tumor cells obtained from resistant tumors were not resistant *in vitro* to JNJ-605 but were able to promote HGF overexpression in CAFs, with the same lactate-based mechanism described for EBC1 cells (FigureS4A-G). Indeed, *in vivo* treatment with the LDH inhibitor NHI-Glc-2 restored the response to JNJ-605 also in RES-J GTL16 tumors (FigureS4H). Moreover, similar results were observed in EBC1 tumors upon acquired resistance to crizotinib, (Figure S5A-F), proving that this mechanism of resistance is not restricted to the JNJ-605 inhibitor.

The lactate-HGF axis mediates adaptive resistance to EGFR TKIs.

In order to understand if the identified non-cell-autonomous mechanism of adaptive resistance could have a wider occurrence, we evaluated if it could mediate TKI resistance in tumors addicted to oncogenes other than MET, and, specifically, in EGFR-addicted lung cancers. The reasons for this choice were many: i) EGFR and MET are biochemically and functionally linked and can frequently compensate for each other (Engelman and Settleman, 2008; Puri and Salgia, 2008); ii) *in vitro* screenings previously demonstrated that HGF is able to confer resistance to EGFR TKIs (Straussman et al., 2012; Wilson et al., 2012), even if the mechanisms underpinning HGF upregulation are unknown; iii) differently from MET inhibitors, EGFR TKIs (erlotinib and gefitinib) are currently used in the clinical practice (Maemondo et al., 2010; Mok et al., 2009; Rosell et al., 2012; Zhou et al., 2011), allowing to evaluate if this mechanism of adaptive resistance is relevant in cancer patients currently candidate for targeted therapies.

To generate *in vivo* tumor models of resistance to erlotinib, mice subcutaneously injected with the human NSCLC HCC827 cell line, bearing deletion of EGFR exon 19 and sensitive to EGFR TKIs, were continuously treated with erlotinib, until resistance onset (RES-E HCC827, Figure 6A). Mice grown without treatment were used as control (WT HCC827). As observed in the MET-addicted models,

tumor cells derived from RES-E HCC827 tumors were not resistant *in vitro* to erlotinib (Figure6B), but resistance was conferred by the conditioned media of CAFs derived from RES-E HCC827 tumors (Figure 6C).These CAFs expressed and released significantly higher levels of HGF compared to WT CAFs (Figure 6D,E). In line with the MET models, RES-E HCC827 tumors relied on a higher glycolytic metabolism (Figure S6A), with increased lactate production compared to WT cells (Figure 6F; moreover, RES-E CAFs showed increased NF-kB levels (Figure 6G). Importantly, LDHA/B silencing (Figure 6H and Figure S6B), MCT4 silencing (Figure 6I and Figure 6SC) or concomitant MET-EGFR inhibition (Figure 6J) effectively restored *in vivo* response to erlotinib in RES-E HCC827 tumors, proving the causative role of the lactate/HGF-induced MET activation in this model of resistance as well.

As observed in the EBC1 model, the metabolic switch in tumor cells could be mimicked *in vitro* by prolonged treatment of HCC827 parental cells with EGFR TKIs, but not by treatment with TKIs targeting other kinases (Figure S6D). The metabolic switch was not due to the selection of a preexisting metabolically different subpopulation, since no population with a stably different glucose-uptake was detected by FACS analysis on HCC827 parental cells (data not shown).

In order to verify whether our results are extendable in other oncogene-addicted lung cancer models, we executed the *in vitro* prolonged treatment in other three lung cancer cell lines, namely HCC4006, PC9 and HCC78. As shown in Figure S6E, in all these cell lines we observed a significant increase of lactate release in response to TKIs targeting the 'driver' oncogene, but not to TKIs targeting unrelated oncogenes. Notably, this was true not only in EGFR-addicted tumor cells (HCC4006 and PC9) but also in the ROS1-addicted lung cancer model (HCC78), suggesting that this mechanism of resistance could be extendable beyond MET- and EGFR- addiction.

Stromal HGF and tumor MCT4 are overexpressed in patients relapsed upon EGFR TKI therapy.

In order to evaluate the clinical relevance of our findings, we investigated whether activation of the lactate/HGF axis may enforce clinical resistance to TKIs. As MET inhibitors are not yet approved for routine clinical use, we focused on patients with EGFR-mutation positive NSCLC and acquired resistance to EGFR TKIs.

We collected paired FFPE tumor samples, obtained at diagnosis and upon resistance onset, of six advanced NSCLC patients with acquired resistance to erlotinib or gefitinib; none of them presented the T790M mutation at relapse. In 5 patients, no classical mechanism of resistance was identified, while in one of them a low grade MET gene amplification had been detected upon progression (Table S1). The samples were analyzed through *in situ* hybridization for human HGF mRNA levels, followed by pan-cytokeratin IHC to differentiate cancer/stroma signal. In 3 out of 6 pairs, we detected a >2-fold increase in the HGF mRNA signal in the tumor stroma upon resistance acquisition (Figure 7A,B). In all the analyzed samples the tumor cells expressed the HGF receptor MET (data not shown).

The same paired samples were also analyzed by IHC for the expression of MCT-4, involved in lactate transport. In both the EBC1 and the HCC827 resistant models, the level of this transporter was increased in resistant cells compared to controls (FiguresS2,S6). In the analyzed NSCLC tumors, MCT4 and HGF expression showed a concordant change upon relapse in 4 out of 6 tumors (Figure 7 and Table S1). To define if MCT4-positive cells were localized within the hypoxic areas of resistant tumors, we performed IHC staining for MCT4 and Carbonic Anhydrase IX (CAIX, a known marker of cell hypoxia) on consecutive slides of the patients' paired biopsies. In the analyzed tumors, the MCT4-positive areas only rarely overlapped with CAIX-positive ones (data not shown), indicating that the upregulation of MCT4 is not linked to hypoxia in this context.

DISCUSSION

Acquired resistance is one of the major limitations to the efficacy of targeted therapies. For this reason, in the last decade, enormous efforts have been made to identify the molecular mechanisms sustaining resistance. Most of the preclinical studies performed so far relied on *in vitro* experiments, carried out in tumor cell lines. In these models, resistance is due to cell-autonomous mechanisms as the therapeutic treatment often selects preexisting clones bearing genetic alterations either in the target itself or in downstream or parallel signaling pathways, eventually compensating for the drug-inhibited kinase. Works performed in these *in vitro* models identified several molecular mechanisms responsible for acquired resistance to tyrosine kinase inhibitors, many of which have been validated in patients (Camidge et al., 2014; Engelman and Settleman, 2008; Lovly and Shaw, 2014) and even clinically exploited as therapeutic targets – as successfully shown for osimertinib in the treatment of NSCLC patients with EGFR T790M-driven acquired resistance to first/second generation EGFR TKIs (Mok et al., 2017). However, *in vitro* models have clear limitations, like the artificial growing conditions and the lack of epithelial-stromal interactions, precluding the identification of non-cell-autonomous mechanisms of resistance. Tumor microenvironment has recently emerged as an important player in sustaining resistance to targeted therapies, for example, through production of ligands that, in a paracrine manner, activate signals able to compensate for the drug-inhibited pathways in tumor cells (Harbinski et al., 2012; Straussman et al., 2012; Wilson et al., 2012). In particular, HGF production by stromal cells has been shown as a mechanism of primary (innate) resistance to TKIs targeting different oncogenes (Straussman et al., 2012; Wilson et al., 2012). In their pivotal work, Straussman and colleagues also reported an increased HGF expression in 5 out of 10 melanoma patients during treatment with BRAF inhibitors (Straussman et al., 2012). However, the mechanism(s) leading to HGF overexpression or its possible occurrence in other tumor types upon different molecular treatments are not known. In general, our knowledge

of non-cell-autonomous mechanisms of resistance is largely incomplete, e.g. it is entirely unknown how tumor cells, undergoing drug treatment, can instruct their microenvironment to activate 'rescue pathways'.

Here we report for the first time that increased lactate production, occurring in cancer cells under TKI treatment, instructs the tumor microenvironment to sustain an adaptive resistance to targeted therapies. In particular, the continuous and prolonged treatment with MET or EGFR TKIs induced an exacerbation of the Warburg metabolism in tumor cells, with increased lactate release. This metabolite led CAFs to increase HGF production, which, in turn, activated MET in cancer cells, overcoming the inhibitory effect of TKIs. Targeting tumor lactate metabolism was sufficient to overcome resistance, thus demonstrating the causative role of the lactate/HGF axis. Importantly, overexpression of stromal HGF and tumor MCT4 was identified in NSCLC patients that acquired resistance to EGFR TKIs, giving a proof of concept of the clinical relevance of our preclinical findings.

A critical concept emerging from this work is that, during the acquisition of drug resistance, a causative expression rewiring may occur not only in cancer cells, but also in the tumor microenvironment: we showed that increased lactate release, due to a metabolic switch induced by drug treatment in cancer cells, is able to increase the expression of lactate transporters, glycolytic enzymes and TCA inhibitors in CAFs and to stably instruct them to overexpress HGF, a cytokine known to protect both normal and cancer cells from apoptosis induced by many stimuli (Carrolo et al., 2003; Pennacchietti et al., 2003; Zeng et al., 2002). It is well established that metabolic plasticity is an effective strategy exploited by cancer cells to counteract environmental or drug-induced stresses (Martinez-Outschoorn et al., 2017). CAFs, one of the major components of tumor microenvironment, profoundly affect metabolic energetics of cancer cells, engaging a symbiotic relationship with them (Bonuccelli et al., 2010; Fiaschi et al., 2012; Martinez-Outschoorn et al., 2014; Salem et al., 2012; Sousa et al., 2016). As recently reported, metabolic coupling between different

cell populations of the tumor, with complementary metabolic profiles, can also sustain the acquisition of resistance to anti-angiogenic treatments (Allen et al., 2016; Jiménez-Valerio et al., 2016; Pisarsky et al., 2016). Végran and colleagues previously showed that lactate is able to induce transcriptional changes in endothelial cells by activating NF-kB, and that this activation requires the production of Reactive-Oxygen–Species (ROS)(Végran et al., 2011). Interestingly, we observed that also in WT CAFs lactate was able to induce ROS upsurge, IkBα degradation and the consequent NF-kB activation (data not shown). The crucial role played by ROS was demonstrated by the inactivation of the lactate/NF-kB axis in the presence of N- acetylcysteine, inhibiting ROS production (data not shown). Thus the lactate-NF-kB-HGF axis described in our work presents several similarities with what observed by Vegran and colleagues in endothelial cells. In both cases, lactate released by cancer cells induced NF-kB activation in non-tumor cells.

An important open question is whether any condition causing a glycolytic switch in tumors (such as hypoxia, or treatment with drugs such as metformin) could lead to acquisition of resistance to TKIs in solid tumors. In preliminary *in vivo* experiments we observed that metformin treatment is not sufficient *per se* to modify the response to TKIs (data not shown). However, the experimental setting (few weeks treatment with TKIs and metformin) is not over-imposable to the one we adopted to generate our models of non-cell-autonomous adaptive resistance. Moreover, in the analyzed human resistant cancer samples we did not find any correlation between HGF production and local hypoxia (data not shown), suggesting that hypoxia is not playing a crucial role in this model of resistance. Future studies are required to comprehensively answer all these questions.

Another key point is that the identified mechanism of adaptive resistance is not based on genetic alterations preexisting in the tumor cells. Recently it has been demonstrated that drug tolerant cells without *bona fide* resistance mechanisms may survive initial drug treatment by epigenetic adaptation and further evolve by acquiring genetic resistance mechanisms (Hata et al., 2016). In line

with this, the lactate/HGF adaptive resistance may represent an intermediate (and possibly reversible) step toward acquisition of a cell-autonomous resistant phenotype, allowing cancer cells to survive initial therapy to generate a reservoir from which the onset of genetic lesions can lead to an irreversible condition of resistance.

Currently, acquired resistance to EGFR TKIs remains unexplained in about one third of *EGFR*-mutation positive NSCLC patients and in a similar proportion of *RAS* and *BRAF* wild-type metastatic colorectal cancer patients receiving anti-EGFR monoclonal antibodies (Pietrantonio et al., 2017). How many of these tumors do rely on the lactate/HGF axis for their survival? The currently analyzed patient series is too small to drive any robust conclusion on its incidence in resistant patients. Remarkably, stromal HGF was reported to induce innate resistance to inhibitors of a range of kinases other than MET and EGFR, such as HER2, FGFR, ALK, PDGFR and BRAF (Straussman et al., 2012; Wilson et al., 2012). Interestingly, we observed lactate increase upon prolonged *in vitro* treatments with ROS1 TKIs in ROS1-addicted cells or HER2 TKIs in HER2-addicted cancer cells (data not shown). These results suggest that the described model of resistance could develop in a broad range of tumors and that it could be extended beyond EGFR- and MET-addiction, further expanding the possible clinical usefulness of our findings.

The fact that increased lactate release can indirectly sustain resistance to different targeted therapies might have profound therapeutic implications. Since tumor lactate levels also correlate with increased metastasis, tumor recurrence and poor outcome, drugs targeting lactate metabolism have been studied in numerous preclinical trials and are now in clinical development (reviewed in (Martinez-Outschoorn et al., 2017)). In particular, LDHA is considered a safe therapeutic target in humans since hereditary loss of LDHA results in mild symptoms of exertional myopathy (Kanno et al., 1988); moreover, MCT1 inhibitors have already entered clinical investigation (NCT01791595). In our work we demonstrated that different players of the lactate axis (both lactate producer and

lactate transporters) are crucial for establishment and maintenance of non-cell-autonomous resistance. These data open new possible applications for LDH, MCT4 and MCT1 inhibitors in preventing/overcoming resistance onset. Alternatively, our data suggest the benefit of combining EGFR TKIs with anti-MET treatments in order to overcome or even prevent resistance onset in a subset of patients not showing MET genetic alterations. In conclusion, our results pave the way for novel combinatorial treatments, simultaneously targeting lactate metabolism -at different levels- and a driver oncogene. Future work is needed to test these therapeutic options, that might show higher long term efficacy and lower probability of resistance onset compared to classical TKI associations.

ACKNOWLEDGMENTS

We thank all our colleagues for helpful scientific discussion; Barbara Martinoglio and Roberta Porporato for providing technical support with Real-time PCR and in situ hybridization; Paola Bernabei for providing technical support with FACS and sorting experiments; Stefania Giove for support with histological preparations; Francesco Fesi for hematochemical analysis; Alberto Puliafito for RNAscope quantification; employees of the animal facility; Dr. Carlos Sebastian for help with metabolic experiments; Dr. Annalisa Petrelli for support in RNAi experiments; Dr. Natale for critical reading of the manuscript. JNJ-605 was kindly provided by Janssen.

This work was funded by the University of Torino, Fondo Ricerca Locale 2013 to S.C.; PROGETTO ATENEO/Compagnia San Paolo 2016, University of Torino to S.C.; the Italian Association for Cancer Research (AIRC), IG grant 15464 to S.G.; Fondazione Piemontese per la Ricerca sul Cancro (ONLUS) 5 X 1000 Fondi Ministero della Salute 2013 to A.S.; M.A. is a recipient of a Fondazione Veronesi Research Fellowship.

AUTHOR CONTRIBUTIONS

Conceptualization:S.G., M.A., S.C., P.C., D.P.

Methodology:M.A, E.G., S.F.,K.J.F.

Investigation and Validation:M.A., E.G., S.F., K.J.F.

Formal Analysis:M.A., E.G., S.F., P.C., E.M., C.I., F.D.

Writing-Original Draft: S.G., M.A., S.C.

Writing-Review and Editing: S.G., M.A., S.C, E.G., S.F., C.I., C.G., F.M., A.S., P.M.C., E.M., F.P., M.V., P.C., K.J.F., D.P., F.D.

Supervision: S.G., S.C.

Resources:C.G., F.M., F.P., M.V.**,** A.S.

Project Administration:S.G., S.C.

Funding Acquisition:S.G., S.C., A.S.

DECLARATION OF INTERESTS

C.G. and F.M. are co-inventors of patents owned by the University of Pisa covering inhibitors of LDH and of cellular lactate production.

REFERENCES

Allen, E., Miéville, P., Warren, C.M., Saghafinia, S., Li, L., Peng, M.W., and Hanahan, D. (2016). Metabolic Symbiosis Enables Adaptive Resistance to Anti-angiogenic Therapy that Is Dependent on mTOR Signaling. Cell Rep *15*, 1144-1160.

Arbiser, J.L., Raab, G., Rohan, R.M., Paul, S., Hirschi, K., Flynn, E., Price, E.R., Fisher, D.E., Cohen, C., and Klagsbrun, M. (1999). Isolation of mouse stromal cells associated with a human tumor using differential diphtheria toxin sensitivity. Am J Pathol *155*, 723-729.

Bacci, M., Giannoni, E., Fearns, A., Ribas, R., Gao, Q., Taddei, M.L., Pintus, G., Dowsett, M., Isacke, C.M., Martin, L.A., et al. (2016). miR-155 Drives Metabolic Reprogramming of ER+ Breast Cancer Cells Following Long-Term Estrogen Deprivation and Predicts Clinical Response to Aromatase Inhibitors. Cancer Res *76*, 1615-1626.

Bhowmick, N.A., Neilson, E.G., and Moses, H.L. (2004). Stromal fibroblasts in cancer initiation and progression. Nature *432*, 332-337.

Bonuccelli, G., Tsirigos, A., Whitaker-Menezes, D., Pavlides, S., Pestell, R.G., Chiavarina, B., Frank, P.G., Flomenberg, N., Howell, A., Martinez-Outschoorn, U.E., et al. (2010). Ketones and lactate "fuel" tumor growth and metastasis: Evidence that epithelial cancer cells use oxidative mitochondrial metabolism. Cell Cycle *9*, 3506-3514.

Bottaro, D.P., Rubin, J.S., Faletto, D.L., Chan, A.M., Kmiecik, T.E., Vande Woude, G.F., and Aaronson, S.A. (1991). Identification of the hepatocyte growth factor receptor as the c-met proto-oncogene product. Science *251*, 802-804.

Calvaresi, E.C., Granchi, C., Tuccinardi, T., Di Bussolo, V., Huigens, R.W., Lee, H.Y., Palchaudhuri, R., Macchia, M., Martinelli, A., Minutolo, F., et al. (2013). Dual targeting of the Warburg effect with a glucose-conjugated lactate dehydrogenase inhibitor. Chembiochem *14*, 2263-2267.

Camidge, D.R., Pao, W., and Sequist, L.V. (2014). Acquired resistance to TKIs in solid tumours: learning from lung cancer. Nat Rev Clin Oncol *11*, 473-481.

Carbone, C., Moccia, T., Zhu, C., Paradiso, G., Budillon, A., Chiao, P.J., Abbruzzese, J.L., and Melisi, D. (2011). Anti-VEGF treatment-resistant pancreatic cancers secrete proinflammatory factors that contribute to malignant progression by inducing an EMT cell phenotype. Clin Cancer Res *17*, 5822-5832.

Carrolo, M., Giordano, S., Cabrita-Santos, L., Corso, S., Vigário, A.M., Silva, S., Leirião, P., Carapau, D., Armas-Portela, R., Comoglio, P.M., et al. (2003). Hepatocyte growth factor and its receptor are required for malaria infection. Nat Med *9*, 1363-1369.

Cecchi, F., Lih, C.J., Lee, Y.H., Walsh, W., Rabe, D.C., Williams, P.M., and Bottaro, D.P. (2015). Expression array analysis of the hepatocyte growth factor invasive program. Clin Exp Metastasis *32*, 659-676.

Cepero, V., Sierra, J.R., Corso, S., Ghiso, E., Casorzo, L., Perera, T., Comoglio, P.M., and Giordano, S. (2010). MET and KRAS gene amplification mediates acquired resistance to MET tyrosine kinase inhibitors. Cancer Res *70*, 7580-7590.

Chong, C.R., and Jänne, P.A. (2013). The quest to overcome resistance to EGFR-targeted therapies in cancer. Nat Med *19*, 1389-1400.

Comoglio, P.M., Giordano, S., and Trusolino, L. (2008). Drug development of MET inhibitors: targeting oncogene addiction and expedience. Nat Rev Drug Discov *7*, 504-516.

Corso, S., Ghiso, E., Cepero, V., Sierra, J.R., Migliore, C., Bertotti, A., Trusolino, L., Comoglio, P.M., and Giordano, S. (2010). Activation of HER family members in gastric carcinoma cells mediates resistance to MET inhibition. Mol Cancer *9*, 121.

Cui, J.J. (2014). Targeting receptor tyrosine kinase MET in cancer: small molecule inhibitors and clinical progress. J Med Chem *57*, 4427-4453.
Curtarello, M., Zulato, E., Nardo, G., Valtorta, S., Guzzo, G., Rossi, E., Esposito, G., Msaki, A., Pastò, A., Rasola, A., et al. (2015). VEGF-targeted therapy stably modulates the glycolytic phenotype of tumor cells. Cancer Res *75*, 120-133.
Dillon, R., Nilsson, C.L., Shi, S.D., Lee, N.V., Krastins, B., and Greig, M.J. (2011). Discovery of a novel B-Raf fusion protein related to c-Met drug resistance. J Proteome Res *10*, 5084-5094.
Engelman, J.A., and Settleman, J. (2008). Acquired resistance to tyrosine kinase inhibitors during cancer therapy. Curr Opin Genet Dev *18*, 73-79.
Fiaschi, T., Marini, A., Giannoni, E., Taddei, M.L., Gandellini, P., De Donatis, A., Lanciotti, M., Serni, S., Cirri, P., and Chiarugi, P. (2012). Reciprocal metabolic reprogramming through lactate shuttle coordinately influences tumor-stroma interplay. Cancer Res *72*, 5130-5140.
Gherardi, E., Birchmeier, W., Birchmeier, C., and Vande Woude, G. (2012). Targeting MET in cancer: rationale and progress. Nat Rev Cancer *12*, 89-103.
Giordano, S., Ponzetto, C., Di Renzo, M.F., Cooper, C.S., and Comoglio, P.M. (1989). Tyrosine kinase receptor indistinguishable from the c-met protein. Nature *339*, 155-156.
Harbinski, F., Craig, V.J., Sanghavi, S., Jeffery, D., Liu, L., Sheppard, K.A., Wagner, S., Stamm, C., Buness, A., Chatenay-Rivauday, C., et al. (2012). Rescue screens with secreted proteins reveal compensatory potential of receptor tyrosine kinases in driving cancer growth. Cancer Discov *2*, 948-959.
Harrison, P.M., and Farzaneh, F. (2000). Regulation of HGF/SF gene expression in MRC-5 cells by N-acetylcysteine. Biochem Biophys Res Commun *279*, 108-115.
Hata, A.N., Niederst, M.J., Archibald, H.L., Gomez-Caraballo, M., Siddiqui, F.M., Mulvey, H.E., Maruvka, Y.E., Ji, F., Bhang, H.E., Krishnamurthy Radhakrishna, V., et al. (2016). Tumor cells can follow distinct evolutionary paths to become resistant to epidermal growth factor receptor inhibition. Nat Med *22*, 262-269.
Hu, Y., Yan, C., Mu, L., Huang, K., Li, X., Tao, D., Wu, Y., and Qin, J. (2015). Fibroblast-Derived Exosomes Contribute to Chemoresistance through Priming Cancer Stem Cells in Colorectal Cancer. PLoS One *10*, e0125625.
Jiménez-Valerio, G., Martínez-Lozano, M., Bassani, N., Vidal, A., Ochoa-de-Olza, M., Suárez, C., García-Del-Muro, X., Carles, J., Viñals, F., Graupera, M., et al. (2016). Resistance to Antiangiogenic Therapies by Metabolic Symbiosis in Renal Cell Carcinoma PDX Models and Patients. Cell Rep *15*, 1134-1143.
Kanno, T., Sudo, K., Maekawa, M., Nishimura, Y., Ukita, M., and Fukutake, K. (1988). Lactate dehydrogenase M-subunit deficiency: a new type of hereditary exertional myopathy. Clin Chim Acta *173*, 89-98.
Lai, I.L., Chou, C.C., Lai, P.T., Fang, C.S., Shirley, L.A., Yan, R., Mo, X., Bloomston, M., Kulp, S.K., Bekaii-Saab, T., et al. (2014). Targeting the Warburg effect with a novel glucose transporter inhibitor to overcome gemcitabine resistance in pancreatic cancer cells. Carcinogenesis *35*, 2203-2213.
Lennerz, J.K., Kwak, E.L., Ackerman, A., Michael, M., Fox, S.B., Bergethon, K., Lauwers, G.Y., Christensen, J.G., Wilner, K.D., Haber, D.A., et al. (2011). MET amplification identifies a small and aggressive subgroup of esophagogastric adenocarcinoma with evidence of responsiveness to crizotinib. J Clin Oncol *29*, 4803-4810.
Lovly, C.M., and Shaw, A.T. (2014). Molecular pathways: resistance to kinase inhibitors and implications for therapeutic strategies. Clin Cancer Res *20*, 2249-2256.
Maemondo, M., Inoue, A., Kobayashi, K., Sugawara, S., Oizumi, S., Isobe, H., Gemma, A., Harada, M., Yoshizawa, H., Kinoshita, I., et al. (2010). Gefitinib or chemotherapy for non-small-cell lung cancer with mutated EGFR. N Engl J Med *362*, 2380-2388.

Martinez-Outschoorn, U.E., Lisanti, M.P., and Sotgia, F. (2014). Catabolic cancer-associated fibroblasts transfer energy and biomass to anabolic cancer cells, fueling tumor growth. Semin Cancer Biol *25*, 47-60.
Martinez-Outschoorn, U.E., Peiris-Pagés, M., Pestell, R.G., Sotgia, F., and Lisanti, M.P. (2017). Cancer metabolism: a therapeutic perspective. Nat Rev Clin Oncol *14*, 113.
Meads, M.B., Gatenby, R.A., and Dalton, W.S. (2009). Environment-mediated drug resistance: a major contributor to minimal residual disease. Nat Rev Cancer *9*, 665-674.
Mok, T.S., Wu, Y.L., Ahn, M.J., Garassino, M.C., Kim, H.R., Ramalingam, S.S., Shepherd, F.A., He, Y., Akamatsu, H., Theelen, W.S., et al. (2017). Osimertinib or Platinum-Pemetrexed in EGFR T790M-Positive Lung Cancer. N Engl J Med *376*, 629-640.
Mok, T.S., Wu, Y.L., Thongprasert, S., Yang, C.H., Chu, D.T., Saijo, N., Sunpaweravong, P., Han, B., Margono, B., Ichinose, Y., et al. (2009). Gefitinib or carboplatin-paclitaxel in pulmonary adenocarcinoma. N Engl J Med *361*, 947-957.
Moore, M.J., Goldstein, D., Hamm, J., Figer, A., Hecht, J.R., Gallinger, S., Au, H.J., Murawa, P., Walde, D., Wolff, R.A., et al. (2007). Erlotinib plus gemcitabine compared with gemcitabine alone in patients with advanced pancreatic cancer: a phase III trial of the National Cancer Institute of Canada Clinical Trials Group. J Clin Oncol *25*, 1960-1966.
Ohashi, K., Maruvka, Y.E., Michor, F., and Pao, W. (2013). Epidermal growth factor receptor tyrosine kinase inhibitor-resistant disease. J Clin Oncol *31*, 1070-1080.
Pennacchietti, S., Cazzanti, M., Bertotti, A., Rideout, W.M., Han, M., Gyuris, J., Perera, T., Comoglio, P.M., Trusolino, L., and Michieli, P. (2014). Microenvironment-derived HGF overcomes genetically determined sensitivity to anti-MET drugs. Cancer Res *74*, 6598-6609.
Pennacchietti, S., Michieli, P., Galluzzo, M., Mazzone, M., Giordano, S., and Comoglio, P.M. (2003). Hypoxia promotes invasive growth by transcriptional activation of the met protooncogene. Cancer Cell *3*, 347-361.
Peters, S., and Adjei, A.A. (2012). MET: a promising anticancer therapeutic target. Nat Rev Clin Oncol *9*, 314-326.
Pietrantonio, F., Vernieri, C., Siravegna, G., Mennitto, A., Berenato, R., Perrone, F., Gloghini, A., Tamborini, E., Lonardi, S., Morano, F., et al. (2017). Heterogeneity of Acquired Resistance to Anti-EGFR Monoclonal Antibodies in Patients with Metastatic Colorectal Cancer. Clin Cancer Res *23*, 2414-2422.
Pisarsky, L., Bill, R., Fagiani, E., Dimeloe, S., Goosen, R.W., Hagmann, J., Hess, C., and Christofori, G. (2016). Targeting Metabolic Symbiosis to Overcome Resistance to Anti-angiogenic Therapy. Cell Rep *15*, 1161-1174.
Puri, N., and Salgia, R. (2008). Synergism of EGFR and c-Met pathways, cross-talk and inhibition, in non-small cell lung cancer. J Carcinog *7*, 9.
Qi, J., McTigue, M.A., Rogers, A., Lifshits, E., Christensen, J.G., Jänne, P.A., and Engelman, J.A. (2011). Multiple mutations and bypass mechanisms can contribute to development of acquired resistance to MET inhibitors. Cancer Res *71*, 1081-1091.
Rosell, R., Carcereny, E., Gervais, R., Vergnenegre, A., Massuti, B., Felip, E., Palmero, R., Garcia-Gomez, R., Pallares, C., Sanchez, J.M., et al. (2012). Erlotinib versus standard chemotherapy as first-line treatment for European patients with advanced EGFR mutation-positive non-small-cell lung cancer (EURTAC): a multicentre, open-label, randomised phase 3 trial. Lancet Oncol *13*, 239-246.
Salem, A.F., Whitaker-Menezes, D., Lin, Z., Martinez-Outschoorn, U.E., Tanowitz, H.B., Al-Zoubi, M.S., Howell, A., Pestell, R.G., Sotgia, F., and Lisanti, M.P. (2012). Two-compartment tumor metabolism: autophagy in the tumor microenvironment and oxidative mitochondrial metabolism (OXPHOS) in cancer cells. Cell Cycle *11*, 2545-2556.

Sequist, L.V., Waltman, B.A., Dias-Santagata, D., Digumarthy, S., Turke, A.B., Fidias, P., Bergethon, K., Shaw, A.T., Gettinger, S., Cosper, A.K., et al. (2011). Genotypic and histological evolution of lung cancers acquiring resistance to EGFR inhibitors. Sci Transl Med *3*, 75ra26.
Shiao, S.L., Ganesan, A.P., Rugo, H.S., and Coussens, L.M. (2011). Immune microenvironments in solid tumors: new targets for therapy. Genes Dev *25*, 2559-2572.
Smolen, G.A., Sordella, R., Muir, B., Mohapatra, G., Barmettler, A., Archibald, H., Kim, W.J., Okimoto, R.A., Bell, D.W., Sgroi, D.C., et al. (2006). Amplification of MET may identify a subset of cancers with extreme sensitivity to the selective tyrosine kinase inhibitor PHA-665752. Proc Natl Acad Sci U S A *103*, 2316-2321.
Sommer, C., Strähle, C., Köthe, U., and Hamprecht, F.A. (2011). ilastik: Interactive Learning and Segmentation

Toolkit. (Eighth IEEE International Symposium on Biomedical

Imaging (ISBI). Proceedings), pp. 230-233
Sousa, C.M., Biancur, D.E., Wang, X., Halbrook, C.J., Sherman, M.H., Zhang, L., Kremer, D., Hwang, R.F., Witkiewicz, A.K., Ying, H., et al. (2016). Pancreatic stellate cells support tumour metabolism through autophagic alanine secretion. Nature *536*, 479-483.
Straussman, R., Morikawa, T., Shee, K., Barzily-Rokni, M., Qian, Z.R., Du, J., Davis, A., Mongare, M.M., Gould, J., Frederick, D.T., et al. (2012). Tumour micro-environment elicits innate resistance to RAF inhibitors through HGF secretion. Nature *487*, 500-504.
Végran, F., Boidot, R., Michiels, C., Sonveaux, P., and Feron, O. (2011). Lactate influx through the endothelial cell monocarboxylate transporter MCT1 supports an NF-κB/IL-8 pathway that drives tumor angiogenesis. Cancer Res *71*, 2550-2560.
Wilson, T.R., Fridlyand, J., Yan, Y., Penuel, E., Burton, L., Chan, E., Peng, J., Lin, E., Wang, Y., Sosman, J., et al. (2012). Widespread potential for growth-factor-driven resistance to anticancer kinase inhibitors. Nature *487*, 505-509.
Yin, J., Lee, J.H., Zhang, J., Gao, Z., Polotsky, V.Y., and Ye, J. (2014). Regulation of hepatocyte growth factor expression by NF-κB and PPARγ in adipose tissue. Am J Physiol Endocrinol Metab *306*, E929-936.
Yu, H.A., Arcila, M.E., Rekhtman, N., Sima, C.S., Zakowski, M.F., Pao, W., Kris, M.G., Miller, V.A., Ladanyi, M., and Riely, G.J. (2013). Analysis of Tumor Specimens at the Time of Acquired Resistance to EGFR-TKI Therapy in 155 Patients with EGFR-Mutant Lung Cancers. Clin Cancer Res.
Zeng, Q., Chen, S., You, Z., Yang, F., Carey, T.E., Saims, D., and Wang, C.Y. (2002). Hepatocyte growth factor inhibits anoikis in head and neck squamous cell carcinoma cells by activation of ERK and Akt signaling independent of NFkappa B. J Biol Chem *277*, 25203-25208.
Zhang, J., and Liu, J. (2013). Tumor stroma as targets for cancer therapy. Pharmacol Ther *137*, 200-215.
Zhou, C., Wu, Y.L., Chen, G., Feng, J., Liu, X.Q., Wang, C., Zhang, S., Wang, J., Zhou, S., Ren, S., et al. (2011). Erlotinib versus chemotherapy as first-line treatment for patients with advanced EGFR mutation-positive non-small-cell lung cancer (OPTIMAL, CTONG-0802): a multicentre, open-label, randomised, phase 3 study. Lancet Oncol *12*, 735-742.
Zhou, M., Zhao, Y., Ding, Y., Liu, H., Liu, Z., Fodstad, O., Riker, A.I., Kamarajugadda, S., Lu, J., Owen, L.B., et al. (2010). Warburg effect in chemosensitivity: targeting lactate dehydrogenase-A re-sensitizes taxol-resistant cancer cells to taxol. Mol Cancer *9*, 33.

FIGURE LEGENDS

Figure 1. *In vivo*-generated tumor adaptive resistance to JNJ-605 is mediated by non-cell-autonomous mechanisms. A. The NSCLC cell line EBC-1 was subcutaneously injected in NOD-SCID mice. When tumors reached a volume > 300 mm^3, 5 mice started a daily treatment with the maximum tolerated dose of the MET inhibitor JNJ-605 until resistance onset (RES-J EBC1 tumors). The growth curves of the resistant tumors and of one representative untreated tumor (WT) are shown. The arrow indicates treatment start. **B.** Cell viability assay (based on ATP content) of EBC1 cells derived from either WT or RES-J EBC1 tumors, treated *in vitro* for 3 days with the indicated increasing concentrations of JNJ-605. **C.** EBC1 cells derived either from a WT or a representative RES-J EBC1 tumor were subcutaneously re-injected in 20 NOD-SCID mice; upon tumor growth, mice were treated either with vehicle or with JNJ-605 (N=5). The arrow indicates treatment start. Tumor growth curves are reported in the graph. **D.** Parental EBC1 cells (sensitive to MET inhibitors) were transduced with a lentiviral vector containing the luciferase cDNA (EBC1 Luc) and $1x10^6$ cells were injected into pre-existing WT or RES-J EBC1 tumors. Mice were treated with JNJ-605 (or with vehicle) for 8 weeks, as indicated in the draw (N=5). The graph represents the luminescence signal of explanted tumors analyzed by IVIS Imaging, as a read out of viable EBC1 Luc cells. **E.** Cell viability assay (based on luciferase signal) performed co-culturing parental EBC1 Luc cells with tumor-derived (murine) CAFs isolated from WT or resistant tumors (WT or RES-J CAFs), in the absence or in the presence of JNJ-605 at the indicated doses. In B,C,D,E data are represented as mean + SD. ** p<0,01; ***p <0,001. On way ANOVA followed by Bonferroni multiple comparisons test has been used for panels D,E; 2way ANOVA multiple comparisons test has been used for panel C.

Figure 2. CAF-increased HGF production is responsible for adaptive resistance to JNJ-605.

A. Cell viability assay (based on cell ATP-content) on parental EBC1 cells treated for 3 days with increasing JNJ-605 concentrations, in the absence or presence of the conditioned media of WT or RES-J CAFs (derived from two different WT or RES-J tumors). **B.** Western Blot analysis of parental

EBC1 cells treated with JNJ-605 (100nM), in the absence or presence of the conditioned media of WT or RES-J CAFs (derived from two different WT or RES-J tumors). Blots have been probed with the indicated antibodies. Vinculin was used as loading control. **C.** qRealTime PCR analysis of mouse HGF mRNA levels in RES-J CAFs compared to WT CAFs. **D.** Elisa assay quantifying the concentration of mouse HGF (mHGF) in the conditioned media of representative WT and RES-J CAFs. **E.** Detection of mouse HGF mRNA by RNA in situ hybridization in representative WT and RES-J CAFs derived in culture (upper panels), in the corresponding original WT vs RES-J EBC1 tumor FFPE slides (medium panels) and in FFPE slides of tumor masses generated upon reinjection in mice of WT vs RES-J EBC1 cells (lower panels). **F.** Cell viability assay on parental EBC1 cells treated for 3 days with JNJ-605 (25nM), in the absence or in the presence of i) WT CAF conditioned medium; ii) RES-J CAF conditioned medium; iii) RES-J CAF conditioned medium upon Heparin-mediated HGF depletion; iv) RES-J CAF conditioned medium upon Heparin-mediated HGF depletion and re-introduction of purified mHGF. **G.** Cell viability assay (based on cell ATP-content) performed culturing parental EBC1 cells with increasing concentrations of JNJ-605 for 3 days, in the absence of any exogenous ligand (blue line) or presence of either purified human HGF (red lines) or murine HGF (green lines), at two different doses. The dashed black line indicates the 50% decrease in cell viability. In panels A,C,D,F,G data are represented as mean + SD**.** * p<0,05; ** p<0,01; *** p<0,001 On way ANOVA followed by Bonferroni multiple comparisons test has been used for panels A, C, D, F.

Figure 3. Lactate-induced metabolic shift drives HGF upregulation in CAFs. A. qRealTime PCR analysis of mouse HGF mRNA levels in WT-CAFs co-cultured with WT-EBC1 or with RES-J EBC1 cells for 1 and 3 weeks. **B.** Enzymatic assay quantifying lactate concentration in the conditioned media of parental EBC1 cells or of two representative WT- and RES-J EBC1 cells **C.** Analysis of [U-14C] glucose uptake in parental, WT or RES-J EBC1 cells. **D.** qRealTime PCR analysis of mouse HGF mRNA levels in WT-CAFs cultured in the presence of increasing concentrations of lactate, up to levels present in

RES-J EBC1 media. **E**. Enzymatic assay quantifying lactate concentration in the conditioned media of representative WT- and RES-J CAFs. **F.**Analysis of [U-14C] glucose uptake in WT or RES-J CAFs. **G.** Heat map of z-score transformed normalized counts of selected genes with GO terms related to glycolysis. **H.** Enzymatic assay quantifying lactate concentration in the conditioned media of parental EBC1 cells treated for four weeks with two different anti-MET TKIs (JNJ-605 or Crizotinib), with a specific AXL inhibitor (TP-0903) or with a specific EGFR TKI (Erlotinib). * p<0,05; ** p<0,01; *** p<0,001. One way ANOVA followed by Bonferroni multiple comparisons test has been used for panels A,B,C,D,I. Two tail student t-test has been used for panels E,F.

Figure 4. HGF transcriptional upregulation in CAFs requires NF-kB. A. Western Blot analysis for IkBα and NFkB levels in WT CAFs stimulated with increasing doses of lactate and in RES-J CAFs, in the absence or in the presence of NF-kB pathway inhibitors (IKK-16 and BMS-345541). Actin was used as loading control. **B.** Elisa assay quantifying the concentration of mouse HGF (mHGF) in conditioned media of WT CAFs stimulated with increasing doses of lactate and of RES-J CAFs, treated with two different NF-kB pathway inhibitors (IKK-16 and BMS-345541) **C.** Cell viability assay (based on cell ATP-content) on parental EBC1 cells treated for 3 days with the IC_{50} concentration of JNJ-605, in the presence of conditioned media derived from: i) WT CAFs; ii) RES-J CAFs; iii) RES-J CAFs pretreated for 72h with the NF-kB pathway inhibitors IKK-16 or BMS-345541; iv) EBC1 pretreated for 72h with the NF-kB pathway inhibitors IKK-16 or BMS-345541 as control .* p<0,05; ** p<0,01; ***p <0,001. In panels B, C data are represented as mean + SD and One way ANOVA followed by Bonferroni multiple comparisons test has been used.

Figure 5. Pharmacologic inhibition or genetic interference of the lactate dehydrogenase enzyme in tumor cells prevent JNJ-605 resistance onset and overcome already established resistance *in vivo*. A. Tumor growth curves of RES-J EBC1 cells subcutaneously reinjected in NOD-SCID mice. Animals (n=5/group) were treated with either vehicle, or JNJ-605 (50 mg/kg), or the LDH inhibitor

NHI-Glc-2 (50mg/kg), alone or in combination (combo). The lines indicate JNJ-605 or NHI-Glc-2 treatment start. **B.** RES-J EBC1 cells transduced either with lentiviral shRNAs targeting the LDH A and LDH B isoforms (two different shRNA pairs) or with a control shRNA were subcutaneously reinjected in NOD-SCID mice and treated with vehicle or JNJ-605 (50 mg/kg) (n=5/group). As control, EBC1 cells obtained from WT tumors were re-injected in mice and treated with vehicle or JNJ-605 (n=5/group). **C.** Three mice shown in Figure 4A (red line), bearing RES-J EBC1 tumors already under treatment with JNJ-605, on day 27 started NHI-Glc-2 treatment as well. The graph shows the tumor growth curve of each mouse. **D.** RES-J EBC1 cells transduced either with lentiviral shRNAs targeting the lactate transporter MCT4 (two different shRNA #1 and #2) or with a control shRNA were subcutaneously reinjected in NOD-SCID mice and treated with vehicle or JNJ-605 (50 mg/kg) (N=6/group) Statistical analysis has been performed on RES-J EBC1 shMCT4 #1;2 JNJ-605 *vs* RES-J EBC1 shCRTL JNJ-605. As control, EBC1 cells obtained from WT tumors were re-injected in mice and treated with vehicle or JNJ-605 (n=3/group). The line indicates - treatment start. **E.** Tumor growth curves of RES-J EBC1 cells subcutaneously reinjected in NOD-SCID mice. Animals were treated with either JNJ-605 (50 mg/kg) or with JNJ-605 plus the MCT1 inhibitor AZD-3965 (100mg/kg) (N=6). Vehicle or AZD-3965 alone were used as control (N=3). The lines indicate JNJ-605 or AZD-3965 treatment start. * p<0,05; ** p<0,01. 2way ANOVA multiple comparisons test has been used The lines indicate JNJ-605 or AZD-3965 treatment start. In panels A,B,D,E data are represented as mean + SD**.** * p<0,05; ** p<0,01 ***<0,001 2way ANOVA multiple comparisons test has been used.

Figure 6. A metabolism-driven, non-cell-autonomous mechanism sustains *in vivo* adaptive resistance to EGFR inhibition in HCC827 lung carcinoma cells. A. The lung carcinoma cell line HCC827 was subcutaneously injected in NOD-SCID mice. When tumors reached a volume >300 mm^3, 3 mice started a daily treatment with the maximum tolerated dose of the EGFR inhibitor erlotinib until the tumors became resistant and grew in the presence of the inhibitor (RES-E HCC827 tumors).

The graph shows the growth curves of the resistant tumors. The arrow indicates treatment start. **B.** *In vitro* cell viability assay of HCC827 cells derived from either WT or RES-E HCC827 tumors, treated for 3 days with increasing concentrations of erlotinib. **C.** Cell viability assay on parental HCC827 cells treated for 3 days with increasing concentrations of erlotinib, in the absence or presence of conditioned media of representative WT or RES-E CAFs (derived from a WT or two different RES-E tumors). **D.** Detection of mouse HGF (mHGF) mRNA by RNA *in situ* hybridization in representative WT and RES-E HCC827 tumor FFPE sections **E.** Elisa assay quantifying the concentration of mouse HGF in conditioned media of two different WT and RES-E CAFs. . **F**. Lactate concentration in the conditioned media of two representative WT and RES-E HCC827 cells. **G.** Western Blot analysis for NF-kB levels in WT and RES-E HCC827 CAFs obtained from HCC827 tumors. Vinculin was used as loading control. **H.** RES-E HCC827 cells transduced either with lentiviral shRNAs targeting the LDH A and LDH B isoforms (two different shRNA pairs) or with a control shRNA were subcutaneously reinjected in NOD-SCID mice and treated with vehicle or erlotinib (50 mg/kg) (N=5/group) Statistical analysis has been performed on RES-E HCC827 shLDHA/B #1;2 ERLOT *vs* RES-E HCC827 shCRTL ERLOT . As control, HCC827 cells obtained from WT tumors were re-injected in mice and treated with vehicle or erlotinib (n=3/group). **I.** RES-E HCC827 cells transduced either with lentiviral shRNAs targeting the lactate transporter MCT4 (two different shRNA #1 and #2) or with a control shRNA were subcutaneously reinjected in NOD-SCID mice and treated with vehicle or erlotinib (50 mg/kg) (N=6/group). Statistical analysis has been performed on RES-E HCC827 shmMCT4 #1;2 ERLOT *vs* RES-E HCC827 shCRTL ERLOT . As control, HCC827 cells obtained from WT tumors were re-injected in mice and treated with vehicle or erlotinib (n=3/group). **J.** Tumor growth curves of HCC827 cells derived from RES-E HCC827 tumors and subcutaneously reinjected in NOD-SCID mice. Animals (n=5/group) were treated with either vehicle, or erlotinib (50 mg/kg), or JNJ-605 (50 mg/kg), alone or in combination (combo). The lines indicate treatment start. N=5/group. In panels B,C,E,F,H,I data

are represented as mean + SD**.*** p<0,05; ** p<0,01; *** p<0,001. One-way ANOVA with Bonferroni multiple comparisons test has been used for panels C, E, F; 2way ANOVA multiple comparisons test has been used for panels H,I,J.

Figure 7. Stromal HGF and tumor MCT4 are increased in NSCLC patients relapsed upon EGFR TKI therapy. **A.** Paired FFPE biopsies of six NSCLC patients (Pt) relapsed after EGFR-TKI treatment were analyzed through *in situ hybridization* (RNAscope) for human HGF, followed by a pan-cytokeratin staining (IHC) to mark tumor cells. The first biopsy was taken at diagnosis (BASAL), the second after EGFT-TKI resistance onset (RESISTANT). The graph shows the percentage of hHGF RNAscope signal in the stroma (data are represented as mean + SD)**.** Below the graph are reported the fold changes of hHGF signal in RESISTANT *versus* BASAL biopsies. **B**. Representative images of paired biopsies of Pt#1 (BASAL and RESISTANT). Upper panels: *In situ hybridization* (RNAscope) for human HGF (red spots), followed by a pan-cytokeratin staining (IHC) to mark the tumor area (brown). Lower panels: IHC staining for the lactate transporter MCT4.

STAR METHODS

CONTACT FOR REAGENT AND RESOURCE SHARING

Further information and requests for resources and reagents should be directed to and will be fulfilled by the Lead Contact, Simona Corso (simona.corso@unito.it).

EXPERIMENTAL MODEL AND SUBJECT DETAILS

Animal Studies

Animal handling and experimentation was performed in accordance with the European Union directives and the Italian Guidelines for Care and Use of Laboratory Animals. All animal procedures were approved by the Ethical Commission of the IRCC in Candiolo and the Italian Ministry of Health. All experiments were performed in 7-8 weeks old female mice NOD SCID mice purchased by Charles River (Milan, Italy) maintained on a 12h light/dark cycle at 22°C. In each animal experiment, mice were randomly assigned to each group.

Cell Culture

The EBC1 (derived from a lung squamous cell carcinoma and purchased from the Japan Cancer Resource Bank), GTL16 (derived from a gastric carcinoma, Smolen et al., 2006),HCC827 (Lung Adenocarcinoma cell line, from ATCC, carrying delE746-A750 and *EGFR* amplification) cell lines were cultured in RPMI medium 1640 (Sigma-Aldrich; Saint Louis, MO,USA) supplemented with 10% fetal bovine serum (FBS), 100 units/mL penicillin, and 100 µg/mL streptomycin.The HCC78 cells (carrying SLC34A2-ROS1 gene rearrangement), were purchased from the Deutsche Sammlung von

Mikroorganismen und Zellkulturen (DSMZ, Braunschweig, Germany) cell bank, The *EGFR* mutant NSCLC (non-small cell lung adenocarcinoma) cell lines HCC4006 (carrying delE746-A750) were obtained from ATCC. Internal batch of PC9 lung adenocarcinoma cells was re-authenticated soon before experimental application.

The genetic identity of the cells has been verified in 2015, 2017 and 2018 by short tandem repeat profiling (Cell ID, Promega, Madison, WI, USA). Mycoplasma testing is performed routinely using the PCR Mycoplasma Detection Kit (Applied Biological Materials Inc., Richmond, BC, Canada). Verified cell lines are generally thawed few weeks before the experiments and kept in culture for 3-6 months. Tumor and CAF cells derived ex-vivo from EBC1, GTL16 and HCC827 xenografts were cultured in RPMI-1640, supplemented as described before.

Patients' tumor FFPE analysis

The study was conducted according to guidelines and regulations by the Research Ethics Committee of the AOU San Luigi/University of Turin and of Fondazione IRCCS Istituto Nazionale dei Tumori, Milan, as explicated by formal approval to M.V and to F.P. of current projects regulating the use of retrospective solid tumor tissues (see Ethics Committee Approvals n.167/2015, prot.17975, 14/11/2015 and n.204/2016, prot.20840, 22/12/2016; protocol INT 117/12). Before the analysis, the samples have been anonymized by staff members of the two hospitals, not involved in the project. No references to the patients can be inferred from the characterization presented in the work.

METHOD DETAILS

Animal tumor models and compounds

$1x10^6$ EBC1/GTL16/HCC827 cells were injected subcutaneously into the right posterior flanks of six week old immunodeficient NOD SCID female mice. When tumors reached a volume of around 200-500 mm^3, mice were treated with JNJ-605 or Crizonitib or Erlotinib at the maximum tolerated dose (50 mg/kg). Both drugs were administrated daily by oral gavages. Tumor size was evaluated weekly by caliper measurements and approximate volume of the mass was calculated using the formula $4/3\ \pi\ (D/2)\ (d/2)^2$, where d is the minor tumour axis and D is the major tumour axis. The MET inhibitor JNJ-605 was provided by Janssen Pharmaceutica NV. Crizotinib (PF-02341066) Erlotinib Mesylate (FE65018) was purchased from Carbosynth (Compton, Berkshire, , UK).

For reinjection experiments, $1x10^6$ EBC1 cells (WT, RES-J, RES-J shCRTL, RES-J shLDHA/B #1, RES-J shLDHA/B #2) and $1x10^6$ GTL16 cells (WT and RES-J), $1x10^6$ HCC827 cells (WT, RES-E, RES-E shCRTL, RES-E shLDHA/B #1, RES-E shLDHA/B #2) were subcutaneously injected into the right posterior flanks of six week old immunodeficient NOD SCID female mice. Mice were treated for the indicated days with the following regimens, (either single agent or in combination): LDH-inhibitor treatment (50 mg/kg) three times a week, by intraperitoneal injection; JNJ-605 (50 mg/kg) daily, ERLOTINIB (50 mg/kg) daily, AZD3965 (100 mg/kg) daily, all of them by oral gavages. Tumour size was evaluated weekly by caliper measurements and approximate volume of the mass was calculated as described before. Experiments were not performed in blind.

Ex-vivo cell cultures

WT and RES-J/C/E EBC1/GTL16/HCC827 cells were derived from tumours after digestion with collagenase 1 (Sigma). After one hour incubation at 37° in a shaking incubator, cells were centrifuged. The pellet was resuspended in L-15 medium (Sigma) supplemented with 10% FBS (Sigma) and cells were incubated for 5 minutes with DNase (Sigma). Cells were washed in L-15 medium, centrifuged and the pellet was resuspended in 5mL red blood cells lysis buffer. After 5 minutes incubation, cells were centrifuged, plated in a cell culture plate and cultured in RPMI-1640,

supplemented as described before. WT and RES-CAF were derived from EBC1, GTL16 and HCC827 tumors as previously described. To obtain pure fibroblast cultures, cells were treated with 10 ng/ml diphtheria toxin (Sigma) for 1 week. Fibroblasts were cultured in RPMI-1640 supplemented as described before.

Cell viability assays

For growth curve and cell viability assay, cells were seeded in triplicates in 96-well culture plates (1500-2000 cells/well), in the presence of drugs. In each well, cells were seeded in 50µl 10% FBS medium and either 100µl of fibroblasts conditioned medium or serum free medium were added. 50 µl of serum free medium containing the drug at the indicated concentrations were added in each well. After 72 hours, cell viability was measured by using Cell Titer-Glo Luminescent Cell Viability Assay (Promega), which directly measures the intracellular ATP content, resulting in quantification of the number of healthy cells in culture.

In vitro co-culture experiments

For the *in vitro* co-culture experiments parental EBC1 cells transduced with a lentiviral vector containing the luciferase cDNA and CAFs derived from wild type or resistant tumors were plated in a 96-well culture plates at 1:3 ratio. Cells were treated for 72h with JNJ-605 at the indicated doses and cell viability was assessed by adding luciferin. The bioluminescent reaction was quantified using VICTOR X Multilabel Plate Readers (PerkinElmer).

In vivo co-culture experiments

Wild type tumors and tumors resistant to treatment with JNJ-605 were generated as described before. When tumors reached a volume of 400 mm^3, $1x10^6$ EBC1 cells transduced with a lentiviral vector containing the luciferase cDNA were inoculated into preformed tumors. Five resistant tumors and five wild type tumors were treated with JNJ-605 at the maximum tolerated dose, while other

five wild type tumors were treated with the vehicle, as controls. JNJ-605 was administrated daily by oral gavages and luciferase signal (from parental sensitive cells) was measured at the end of the experiment (6 weeks) using IVIS Spectrum (PerkinElmer). Experiments were not performed in blind.

CAF treatment with exogenous lactate

WT CAFs ($1,5x10^6$ cells/$60cm^2$ culture dishes) were grown in complete medium for 24h and then serum-starved and treated with increasing concentrations of sodium L-Lactate (#71718 Sigma-Aldrich) for 72 h.

Treatment with NF-kB inhibitors

WT and RES-J CAFs were treated with 1uM of IKK-16 (Santa Cruz) and 1uM BMS-345541 (SIGMA) for 48h, in presence or in absence of Lactate as described before. After that, murine-HGF concentration in cell culture supernatants was quantified through the ELISA assay. For cell viability assay on EBC1 cells confluent RES-J CAFs or EBC1 cells were treated with 1uM of NF-kB inhibitors for 72h and then the media were collected and used on the parental EBC1 for the cell viability assay.

Protein extraction and Western blot

For Western blot analysis, cells were plated in 6-well plates, allowing them to reach 50-60% confluence. Cells were grown in the presence of 10% FBS RPMI medium, conditioned medium of wild type fibroblasts or supernatant of resistant fibroblasts (obtained as described before) for one night. MET-TKI JNJ-605 was added 80min before cell lysis. Cells were lysed in LB buffer [2% SDS, 0.5 mol/L Tris-HCl (pH 6,8)]. Protein concentration of whole-cell lysates was evaluated with the BCA Protein Assay Kit (Pierce). Western blots were performed according to standard methods. The primary antibodies used were as follows: phosphorylated Met ($Tyr^{1234/1235}$) (Clone D26), phosphorylated ERK (Thr^{202}/Tyr^{204}), phosphorylated AKT (Ser^{473}) (Clone D9E), total AKT, total ERK, Hexokinase II (#2867), GLUT1 (#12939), LDHA (#2012), all from Cell Signalling (LEIDEN,

NETHERLANDS). Total MET (clone C28), MCT4 (#sc-50329), IkBα (#sc-371), total NFkB (#sc-8008), LDHB (Q-21), ACTIN were from Santa Cruz Biotechnology (California, USA). Vinculin (1931) was from Sigma. Secondary antibodies were from Amersham (MILANO-ITALY). Detection was performed with ECL system (Amersham) and the final signal detection was done with enhanced chemioluminescence system (Amersham Pharmacia).

Cell Transduction

Parental EBC1 cells ($1x10^6$ cells/100 mm plate) were stably transduced using 40 ng/ml of p24 of lentiviral particles encoding for luciferase cDNA. Luciferase transduction was tested by evaluating luciferase signal. The bioluminescent reaction was quantified using VICTOR X Multilabel Plate Readers (PerkinElmer)

RES-J EBC1 and RES-E HCC827 cells were stably genetically interferenced with 40 ng/ml of p24 lentiviral vector particles encoding for shCRTL RNA, or for 2 couples of LDHA (TRCN0000026-541/554) and LDHB shRNAs (TRCN0000028-488/502; SIGMA), or for 2 different MCT4 shRNAs (TRCN0000038476/586/589; SIGMA).

FACS and SORTING analysis

Immunofluorescence staining was performed on plasma-membrane bound EpCAM on EBC1 cell line, RES-J EBC1 cells and CAF ($2x10^5$). Fluorescence intensity was measured by cytofluorimetric analysis (FACS analysis, CyAn ADP, Beckman Coulter s.r.l.) and analyzed using Summit Software 4.3. For the assay, cells were trypsinized, washed with PBS 2% FBS and stained with the EpCAM-FITC antibody (Miltenyi Biotec) for 20 minutes at room temperature. As negative control, cells were stained with a control IgG1-FITC antibody (Alexa Fluor).

For the glucose uptake assays cells were grown under normal conditions for 24 hr and 100 μM 2-NBDG (Invitrogen) was added to the media for 2 hours. The two gaussian tails (corresponding to the

most and least glycolytic cells) were sorted (MoFlo ASTRIOS EQ di Beckman Coulter) and kept in culture. After one week cells were analysed again for glucose uptake through NBDG staining on FACS Cyan (CyAn ADP, Beckman Coulter s.r.l.) and analyzed using Summit Software 4.3.

ELISA assays

Mouse Hepathocyte Growth Factor concentration was quantified in cell culture supernatants using Quantikine ELISA (R&D System; McKinley, MN, USA) according to the manufacturer's protocol. Optical density was determined using a microplate reader set to 450 nm.

Gene expression analysis by real-time PCR

mRNA extracted using the Trizol (Thermofisher, WALTHAM, MA, USA), following the manufacturer instructions, was reverse transcribed into cDNA using the High Capacity cDNA Reverse Transcription Kit (Thermofisher, WALTHAM, MA, USA) and random primers according to the manufacturer's protocol; cDNA was amplified by Real-time qPCR using the Power SYBR Green PCR Master Mix, according to the manufacturer's protocol (Thermofisher). Real-time qPCR was performed in triplicates using the following primers: mHGF (mouseHGF) and m-Actin (mouseACTIN) (SYBR®Green, sequence are available on request). Gene expression was determined by ΔΔCT method.

RNA in situ hybridization and IHC analysis

The RNAscope probe for mouse HGF (Mm-Hgf-O1 #435381, Advaced Cell Diagnostics) was hybridized on 4 µm FFPE slides of WT/RES-J CAF and WT/ RES-J tumors following the RNAscope 2.5RED assay protocol (#322452 and #322360). Sequential slides were stained with a mouse-specific control probe (mmPPIB: Peptidyl-prolyl cis-trans isomerase B, not shown).

The RNAscope probe for human HGF (Hs-HGF-C2 #310761 Advaced Cell Diagnostics) was hybridized on 4 µm FFPE slides of BASAL and RESISTANT biopsies (taken before and after the treatment with

anti-EGFR therapy) of six different patients with NCSLC. After that, the same slides have been hybridized, through immunohistochemistry experiment, with anti-Human cytokeratin antibody (CloneAE1/AE3 #M3515-DAKO Glostrup Denmark) following the standard protocol. Immunohistochemistry for MCT4 was performed on a sequential 4 μm thick tissue section using the MCT4 antibody (#sc-50329-Santa Cruz Biotechnology).

LDH inhibitor production

LDH inhibitor NHI-Glc-2 was synthesized as previously reported (Calvaresi et al., 2013), starting from commercially available precursors which were purchased from commercial suppliers (Sigma-Aldrich, Alfa Aesar/ Thermo Fisher Scientific Inc., Ricci Chimica) and used without further purification. Briefly, the synthesis started from 2-methyl-3-nitrobenzotrifluoride, which was treated with *N*-iodosuccinimide (NIS) in H_2SO_4. The resulting iodo-derivative was subjected to a Pd-catalyzed cross-coupling reaction with phenylboronic acid. The following biphenyl derivative was transformed into a ketoester intermediate in the presence of potassium *tert*-butoxide and dimethyl oxalate. A subsequent reductive cyclization step with $SnCl_2$ in DME produced the *N*-hydroxyindole methyl ester. This compound was then condensed with a tetra-acetylated glucose moiety. Final deprotection of the hydroxyl groups with sodium methoxide in methanol produced NHI-Glc-2.

Chromatin Immunoprecipitation (ChIP) and Antibodies

Chromatin immunoprecipitation (ChIP) analyses were performed with the following antibodies: rabbit anti-H3 (Abcam, Cat. 1791), rabbit anti-H3K4me1 (Abcam, Cat. 8895), rabbit anti-H3K4me3 (Active Motif, Cat. 39159), rabbit anti-H3K27me3 (Cell Signaling, Cat. 9733), rabbit anti-H3K27ac (Active Motif, Cat. 39133), rabbit anti-H3K36me3 (Cell Signaling, Cat. 4909), rabbit anti-H3K9me3 (Abcam, Cat. 8898). Rabbit IgG (Sigma, Cat. I5006) was used as negative control in ChIP and ChIP assays were carried out as described previously (Pasini et al., 2010). Briefly, 1% formaldehyde cross-

linked chromatin was fragmented by sonication to an average size of 300–500bp and incubated overnight in IP Buffer (33 mM Tris/HCl, pH 8, 100 mM NaCl, 5 mM EDTA, 0.2% NaN3, 0.33% SDS, 1.66% Triton X-100) at 4 ºC with 3 µg of the indicated antibodies, followed by incubation for 2 hr with protein A sepharose beads (GE Healthcare). Beads were washed three times with 150 washing buffer (20 mM Tris/HCl, pH 8, 150 mM NaCl, 2 mM EDTA, 0.1% SDS, 1 % Triton X-100), once with 500 washing buffer (20 mM Tris/HCl, pH 8, 500 mM NaCl, 2 mM EDTA, 0.1% SDS, 1% Triton X-100), and finally re-suspended in 120 µl of de-crosslinking solution (0.1 M NaHCO3, 1% SDS).

RNA sequencing

mRNA-seq library preparation from 4 µg of total RNA was performed with TruSeq RNA Sample Prep Kit V2 (Illumina) according to the manufacturer's instructions.

RNA-seq was carried out using the SMART-seq2 protocol (PMID:24385147) with minor modifications. Briefly, the poly-A containing mRNA molecules from 5 ng of total RNA were copied into first strand cDNA by reverse transcription and template-switching using oligo(dT) primers and an LNA-containing template-switching oligo (TSO). The resulting cDNA was pre-amplified, purified and tagmented with Tn5 transposase produced in-house using a described protocol (PMID:25079858). cDNA fragments generated after tagmentation were gap-repaired, enriched by PCR and purified to create the final cDNA library. Sequencing was carried out in a HiSeq 2000, single end mode, 50bp.

RNA-seq analysis

Demultiplexing was performed using bcl2fastq v2.19. Reads were aligned to mm9 genome using tophat (v2.1.1) with parameters --no-coverage-search --library-type fr-unstranded. Then, PCR duplicates were removed using picardTools (v1.62) (http://broadinstitute.github.io/picard/) and

read counts per gene were calculated using Htseq-count (v0.7.2) (PMID:25260700) with parameters -q -t exon --stranded=no --mode=intersection-nonempty. Genes with 0 counts in all samples were removed and differential expression analysis was performed using DESeq2 (v3.7) (PMID:25516281) with default parameters. Genes with an absolute log2FC >= 2 and FDR <= 0.1 were considered as differentially expressed. The list of upregulated and downregulated genes were loaded into Enrichr (PMID:27141961) to perform gene set enrichment analysis. Finally, read counts were transformed using rlog function (regularized logarithmic transformation) from DESeq2 and then transformed to Z-score for heatmap representation.

QUANTIFICATION AND STATISTICAL ANALYSIS

Stromal hHGF RNAscope signal quantification

To quantify the amount of positive RNAscope regions in the stromal (pan-cytoketarin negative) areas, 5 digital images/slide have been captured at 20x magnification. We performed image segmentation by means of Ilastik (Sommer et al., 2011). Briefly Ilastik was trained to recognize RNAscope positive regions (red hue regions), nuclei (blue hue stained for with hematoxylin), tumor cells (brown hue stained for pan-cytokeratin) and background. Once trained, the algorithm was applied to all images in the dataset. The output of Ilastik was a set of labeled images, which were post-processed as follows: holes in nuclei regions were filled; tumor and nuclei boundaries were smoothed by morphological closing. Segmented nuclei were filtered for size, in order to remove small segmentation leftovers. RNAscope positive regions enclosed within tumor regions were excluded from the computation and nuclei enclosed into brown regions were considered as tumor and therefore excluded from the analysis. The total image area corresponding to nuclei or RNAscope

positive regions was computed. The amount of RNAscope positive divided by the total stromal nuclei area blue plus red area was used as a proxy of the amount of stromal HGF. Post-processing and area fraction calculation was performed thanks to a custom-written Matlab (The Mathworks) algorithm. Both images capture and their analysis have been performed blind by two different people.

Images were captured with the AxiovisionLe software (Zeiss, Gottingen, Germany) using an Axio Zeiss Imager 2 microscope (Zeiss, Gottingen, Germany). MCT4 staining was scored blind by the pathologist using the H-score which is based on the intensity of the signal and on the percentage of cells stained, and results in a score ranging from 0 to 300.

Statistical Analysis

Statistical testing was performed with GraphPAD PRISM Software 7.02, using OneWayAnova with Bonferroni's multiple comparisons, or T-TEST. For in vivo experiments, 2wayANOVA with Bonferroni's multiple comparisons test has been used, as indicated in Figure Legends. Error bars in the figures represent the SD. Statistical significance:*p <0,05; **p <0,01; ***p <0,001.

KEY RESOURCES TABLE

REAGENT or RESOURCE	SOURCE	IDENTIFIER
Antibodies		
EpCAM FITC (CD326)	Miltenyi Biotec	Cat#130-080-301
IgG1-FITC	Alexa Fluor	Cat#551954
phosphorylated Met ($Tyr^{1234/1235}$) (Clone D26)	Cell Signalling	Cat#3077
phosphorylated ERK ($Thr^{202}/Tyr^{204)}$	Cell Signalling	Cat#9101
phosphorylated AKT (Ser^{473}) (Clone D9E)	Cell Signalling	Cat#4060
total AKT	Cell Signalling	Cat#9272
total ERK	Cell Signalling	Cat#9102
Hexokinase II	Cell Signalling	Cat#2867
GLUT1	Cell Signalling	Cat#12939

LDHA	Cell Signalling	Cat#2012
Total MET (clone C28)	Santa Cruz Biotechnology	Cat#sc-161
MCT4	Santa Cruz Biotechnology	Cat#sc-50329
IkBα	Santa Cruz Biotechnology	Cat#sc-371
total NFkB	Santa Cruz Biotechnology	Cat#sc-8008
LDHB (Q-21)	Santa Cruz Biotechnology	Cat#sc-133731
Vinculin	Sigma	Cat#v9131
ACTIN	Santa Cruz Biotechnology	Cat#sc-1616
phospho-EGFR (Y1068)	Abcam	Cat #5644
total EGFR	Santa Cruz Biotechnology	Cat#sc-71033
anti-Human cytokeratin CloneAE1/AE3	DAKO	Cat#M3515
rabbit anti-H3 rabbit	Abcam	Cat#1791
rabbit anti-H3K4me1	Abcam	Cat#8895
anti-H3K4me3	Active Motif	Cat#39159
rabbit anti-H3K27me3	Cell Signaling	Cat#9733
rabbit anti-H3K27ac	Active Motif	Cat#39133
rabbit anti-H3K36me3	Cell Signaling	Cat#4909
rabbit anti-H3K9me3	Abcam	Cat#8898
rabbit IgG	Sigma	Cat#I5006
Biological Samples		
Human Lung Carcinoma FFPE slides	AOU San Luigi/University of Turin and of Fondazione IRCCS Istituto Nazionale dei Tumori, Milan	
Chemicals, Peptides, and Recombinant Proteins		
JNJ-38877605	Janssen Pharmaceutica	NA
Crizotinib	Carbosynth	Cat#PF-02341066
Erlotinib Mesylate	Carbosynth	Cat#FE65018
LDHA inhibitor - NHI-Glc-2	Calvaresi et al., 2013	NA
L-Lactate	Sigma-Aldrich	Cat#71718
2-NBDG	Invitrogen	Cat#N13195
IKK-16	Selleckchem	Cat#S2882
BMS-345541	Selleckchem	Cat#S8044
Oxamate LDH inhibitor	Sigma Aldrich	Cat#02751
MCT1-i (Monocarboxylate transporter 1 inhibitor)	TOCRIS	Cat# AR-C155858
AZD3965	Carbosynth	Cat#BA164976
diphtheria toxin	Sigma Aldrich	Cat# D0564
Critical Commercial Assays		
Quantikine ELISA murine HGF	R&D System	Cat#MHG00
Cell Titer-Glo Luminescent Cell Viability Assay	Promega	Cat#G7573
miRNeasy Mini Kit	Qiagen	Cat#217004

High Capacity cDNA Reverse Transcription Kit	Thermofisher	Cat#4368814
Power SYBR Green PCR Master Mix	Thermofisher	Cat#a10315
RNAscope 2.5 RED protocol	Advaced Cell Diagnostics	Cat.#322452 Cat.#322360
BCA Protein Assay Kit	Pierce	Cat#23225
ECL system	Amersham	Cat#1015
Lactate Assay kit	BioVision	Cat#K607-100
Experimental Models: Cell Lines		
Human EBC1 lung squamous carcinoma cell line	Japanese cancer resource bank	NA
Human HCC827 adenocarcinoma cell line	ATCC	NA
Human GTL16 gastric cancer cell line	Smolen et al., 2006	NA
Ex vivo derived murine CAFs	this paper	NA
Human PC-9 Lung cancer cell line	From IRCCs-Candiolo	NA
Human H4006 Lung Adenocarcinoma cell line	ATCC	NA
Human HCC-78 Lung cancer cell line	Deutsche Sammlung von Mikroorganismen und Zellkulturen (DSMZ, Braunschweig, Germany)	NA
Experimental Models: Organisms/Strains		
Mouse: NOD SCID	Charles River (Milan, Italy	Charles River:NOD.CB17-Prkdcscid/NCrCrl
Oligonucleotides		
HGF Mm-Hgf-O1	Advanced Cell Diagnostics	Cat#435381
Hs-HGF-C2	Advanced Cell Diagnostics	Cat#310761
LDHA shRNAs	Sigma	Cat#TRCN0000026-541/554
LDHB shRNAs	Sigma	Cat#TRCN0000028-488/502
MCT4 shRNAs	Sigma	Cat#TRCN0000038476/589
mHGF (mouse HGF)	SYBR®Green	This paper
m-Actin (mouse ACTIN)	SYBR®Green	This paper
m-HPRT	Applied Biosystems	Cat#mm00446968m1
m- Slc16a1	Applied Biosystems	Cat#mm01306379m1

Mouse Slc16a1 (20501) siRNA-SMARTpool	Dharmacon	Cat#L-058863-01-0005
Deposited data		
Software and Algorithms		
AxiovisionLe software	Zeiss	NA
Matlab (The Mathworks) algorithm		NA
Ilastik algorithm	Sommer et al., 2011	NA

Figure 1

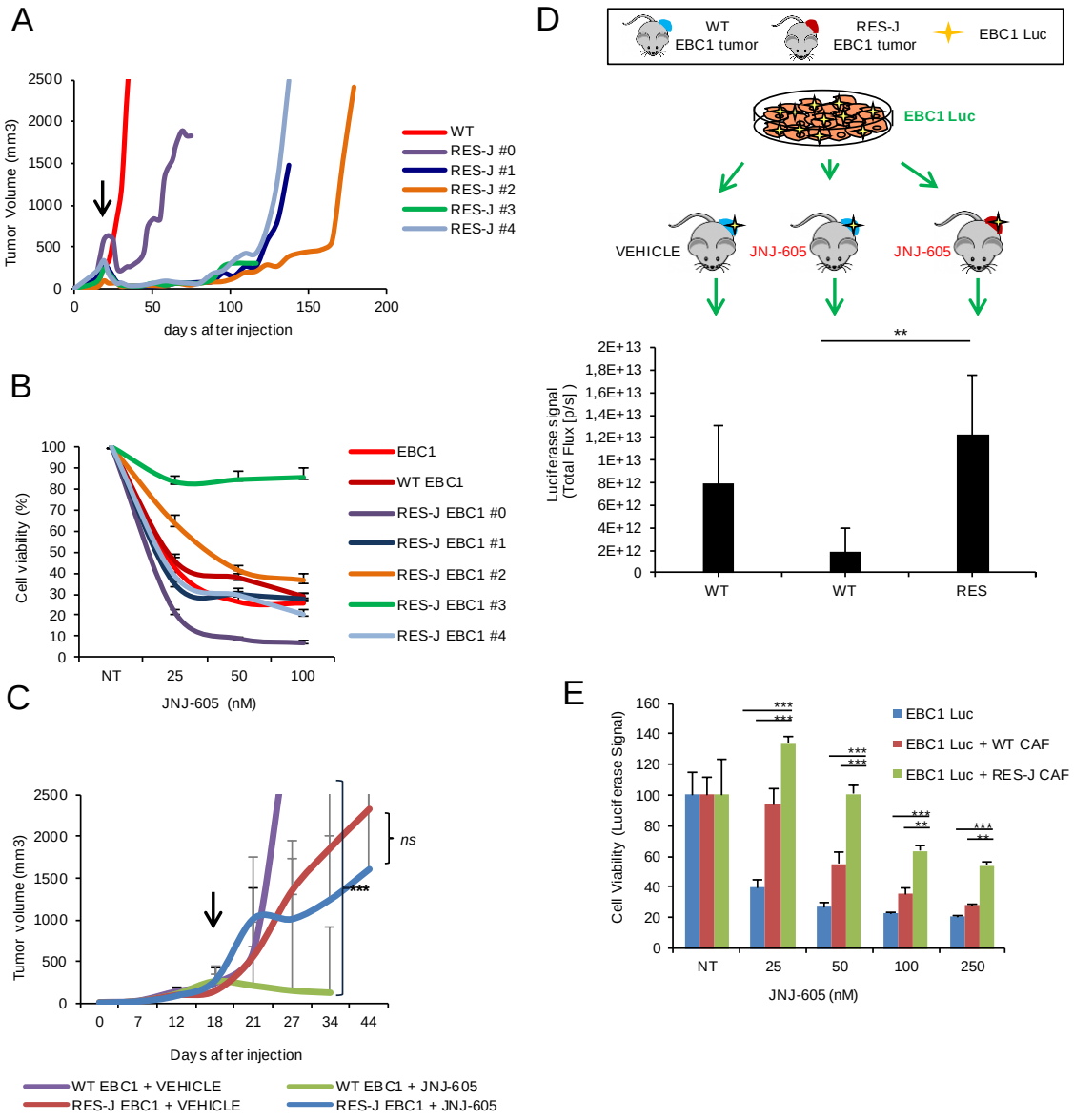
A
Tumor Volume (mm3)
days after injection
WT
RES-J #0
RES-J #1
RES-J #2
RES-J #3
RES-J #4
B
Cell viability (%)
JNJ-605 (nM)
EBC1
WT EBC1
RES-J EBC1 #0
RES-J EBC1 #1
RES-J EBC1 #2
RES-J EBC1 #3
RES-J EBC1 #4
C
Tumor volume (mm3)
Days after injection
ns
WT EBC1 + VEHICLE
RES-J EBC1 + VEHICLE
WT EBC1 + JNJ-605
RES-J EBC1 + JNJ-605
D
WT EBC1 tumor
RES-J EBC1 tumor
EBC1 Luc
VEHICLE
JNJ-605
JNJ-605
Luciferase signal (Total Flux [p/s])
WT
WT
RES
E
Cell Viability (Luciferase Signal)
JNJ-605 (nM)
EBC1 Luc
EBC1 Luc + WT CAF
EBC1 Luc + RES-J CAF

Figure2

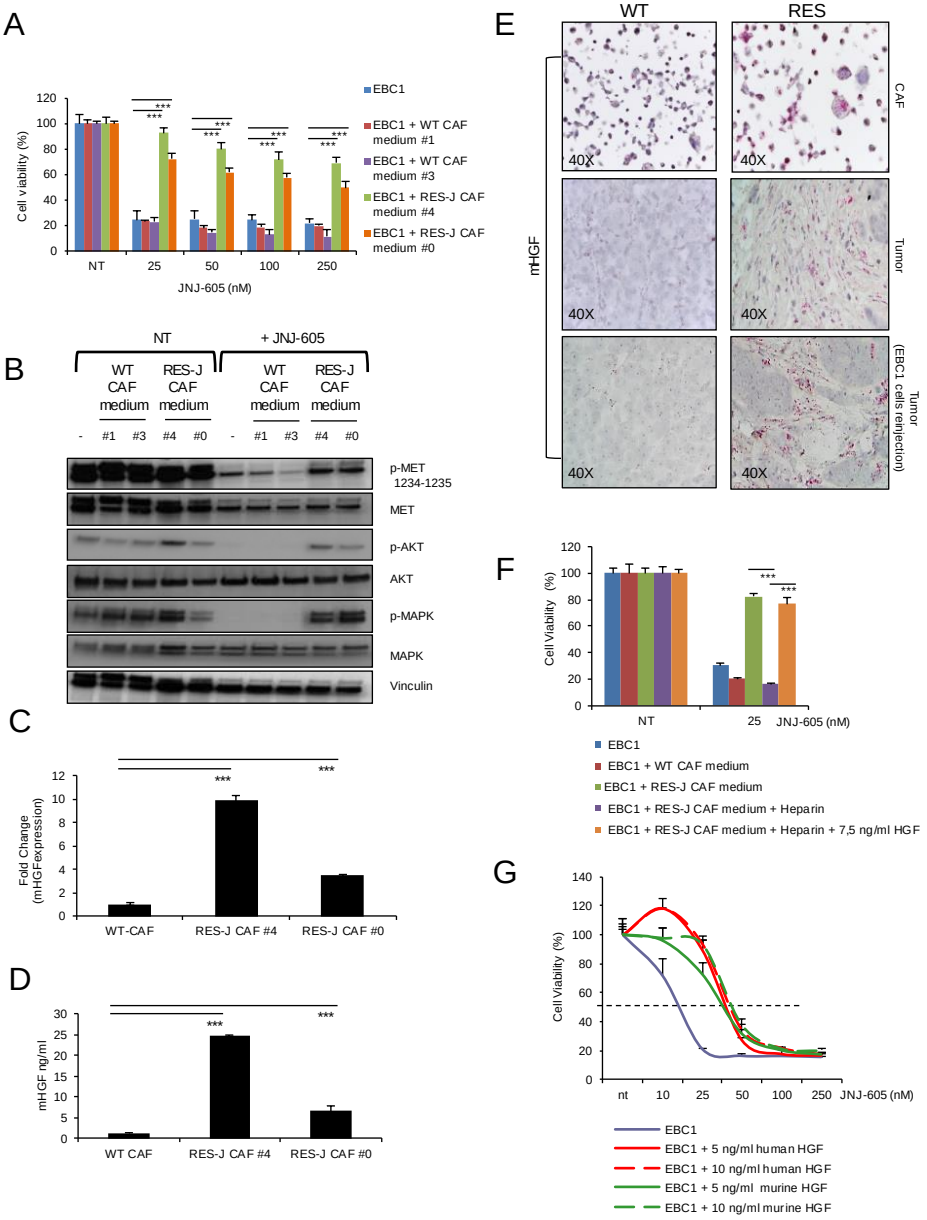
A
Cell viability (%)
JNJ-605 (nM)
NT
25
50
100
250
EBC1
EBC1 + WT CAF medium #1
EBC1 + WT CAF medium #3
EBC1 + RES-J CAF medium #4
EBC1 + RES-J CAF medium #0
B
NT
+ JNJ-605
WT CAF medium
RES-J CAF medium
p-MET 1234-1235
MET
p-AKT
AKT
p-MAPK
MAPK
Vinculin
C
Fold Change (mHGFexpression)
WT-CAF
RES-J CAF #4
RES-J CAF #0
D
mHGF ng/ml
WT CAF
RES-J CAF #4
RES-J CAF #0
E
WT
RES
mHGF
CAF
Tumor
Tumor (EBC1 cells reinjection)
40X
F
Cell Viability (%)
NT
25
JNJ-605 (nM)
EBC1
EBC1 + WT CAF medium
EBC1 + RES-J CAF medium
EBC1 + RES-J CAF medium + Heparin
EBC1 + RES-J CAF medium + Heparin + 7,5 ng/ml HGF
G
Cell Viability (%)
nt
10
25
50
100
250
JNJ-605 (nM)
EBC1
EBC1 + 5 ng/ml human HGF
EBC1 + 10 ng/ml human HGF
EBC1 + 5 ng/ml murine HGF
EBC1 + 10 ng/ml murine HGF

Figure 3

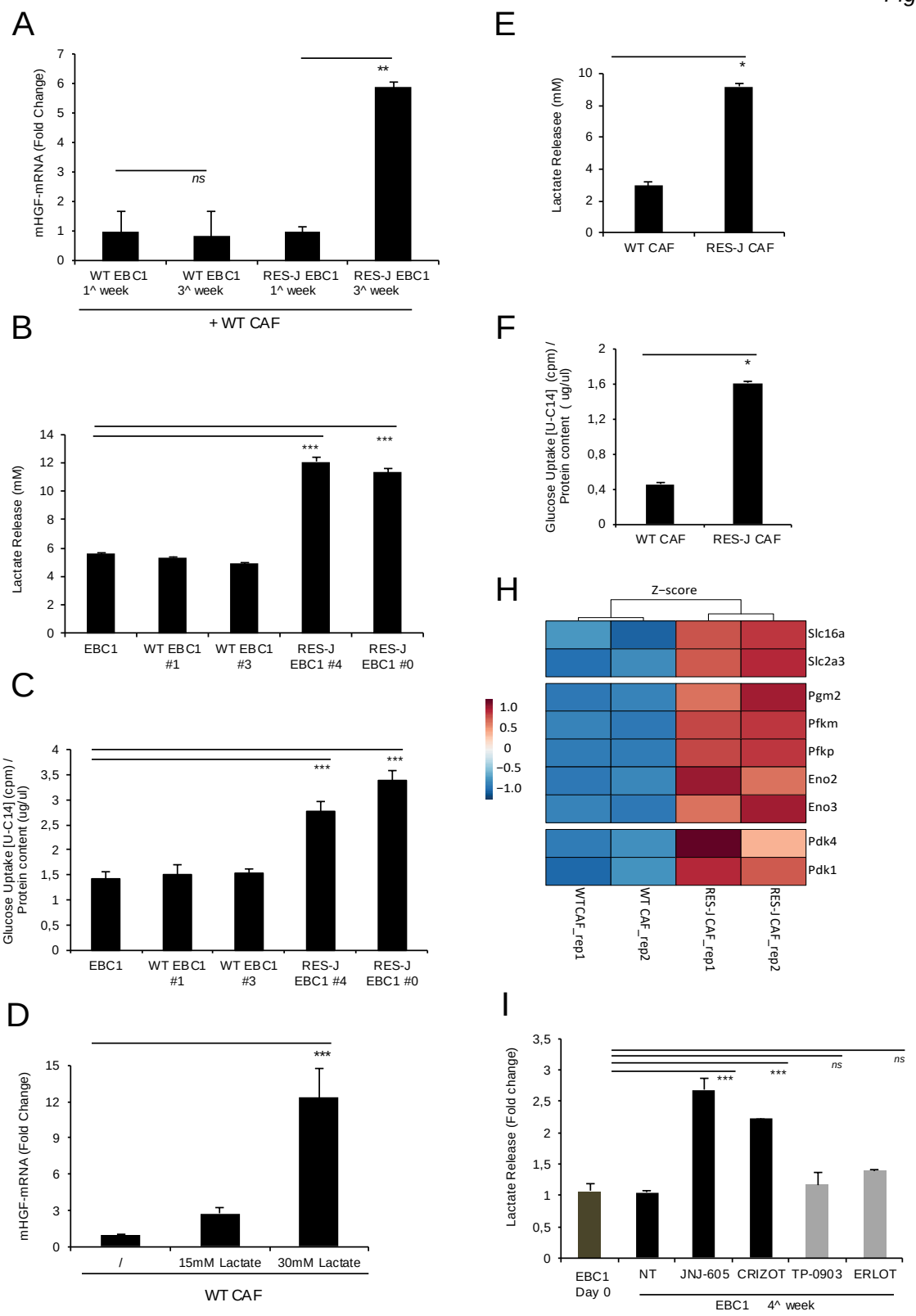
A
mHGF-mRNA (Fold Change)
ns
**
WT EBC1 1^ week
WT EBC1 3^ week
RES-J EBC1 1^ week
RES-J EBC1 3^ week
+ WT CAF
B
Lactate Release (mM)
***
***
EBC1
WT EBC1 #1
WT EBC1 #3
RES-J EBC1 #4
RES-J EBC1 #0
C
Glucose Uptake [U-C14] (cpm) / Protein content (ug/ul)
***
***
EBC1
WT EBC1 #1
WT EBC1 #3
RES-J EBC1 #4
RES-J EBC1 #0
D
mHGF-mRNA (Fold Change)
***
/
15mM Lactate
30mM Lactate
WT CAF
E
Lactate Releasee (mM)
*
WT CAF
RES-J CAF
F
Glucose Uptake [U-C14] (cpm) / Protein content (ug/ul)
*
WT CAF
RES-J CAF
H
Z-score
1.0
0.5
0
−0.5
−1.0
Slc16a
Slc2a3
Pgm2
Pfkm
Pfkp
Eno2
Eno3
Pdk4
Pdk1
WTCAF_rep1
WT CAF_rep2
RES-J CAF_rep1
RES-J CAF_rep2
I
Lactate Release (Fold change)
ns
ns
***
***
EBC1 Day 0
NT
JNJ-605
CRIZOT
TP-0903
ERLOT
EBC1 4^ week

Figure 4

A

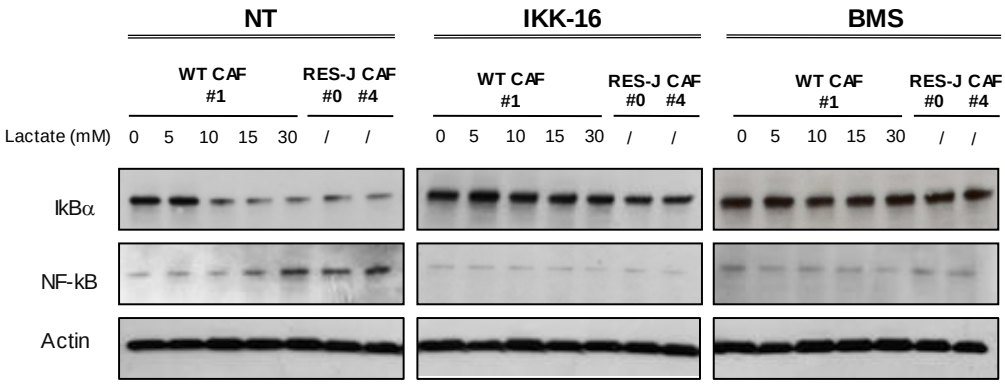
NT
IKK-16
BMS
WT CAF #1
RES-J CAF #0 #4
Lactate (mM)
0 5 10 15 30 / /
IkBα
NF-kB
Actin

B

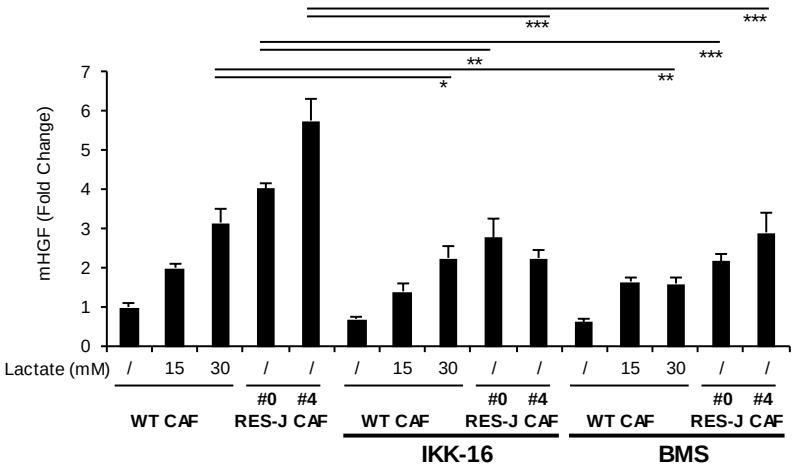
mHGF (Fold Change)
Lactate (mM)
/ 15 30 / /
WT CAF
#0 #4
RES-J CAF
IKK-16
BMS
*
**
***

C

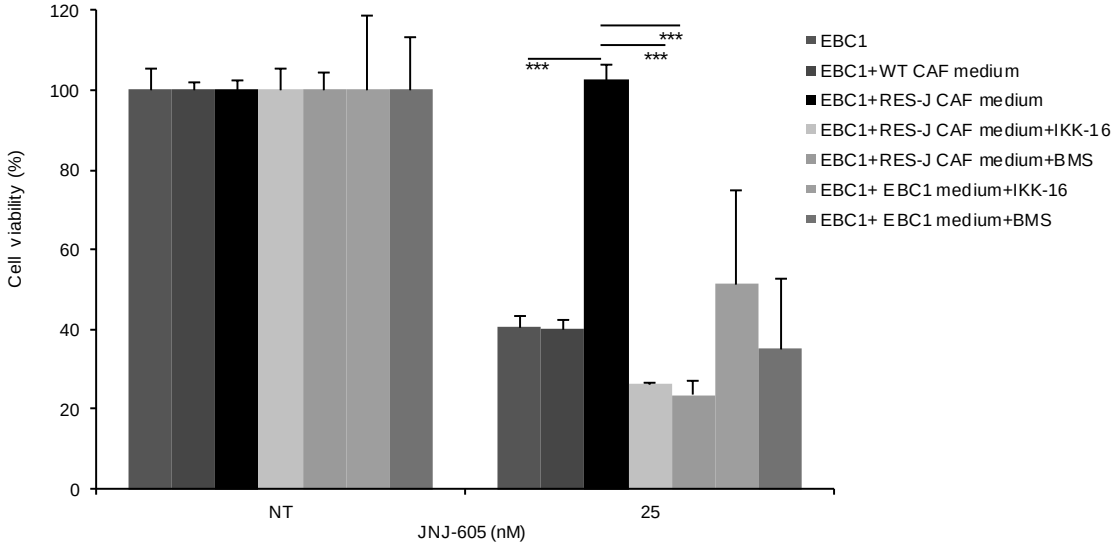
Cell viability (%)
JNJ-605 (nM)
NT
25
EBC1
EBC1+WT CAF medium
EBC1+RES-J CAF medium
EBC1+RES-J CAF medium+IKK-16
EBC1+RES-J CAF medium+BMS
EBC1+ EBC1 medium+IKK-16
EBC1+ EBC1 medium+BMS
***

Figure 5

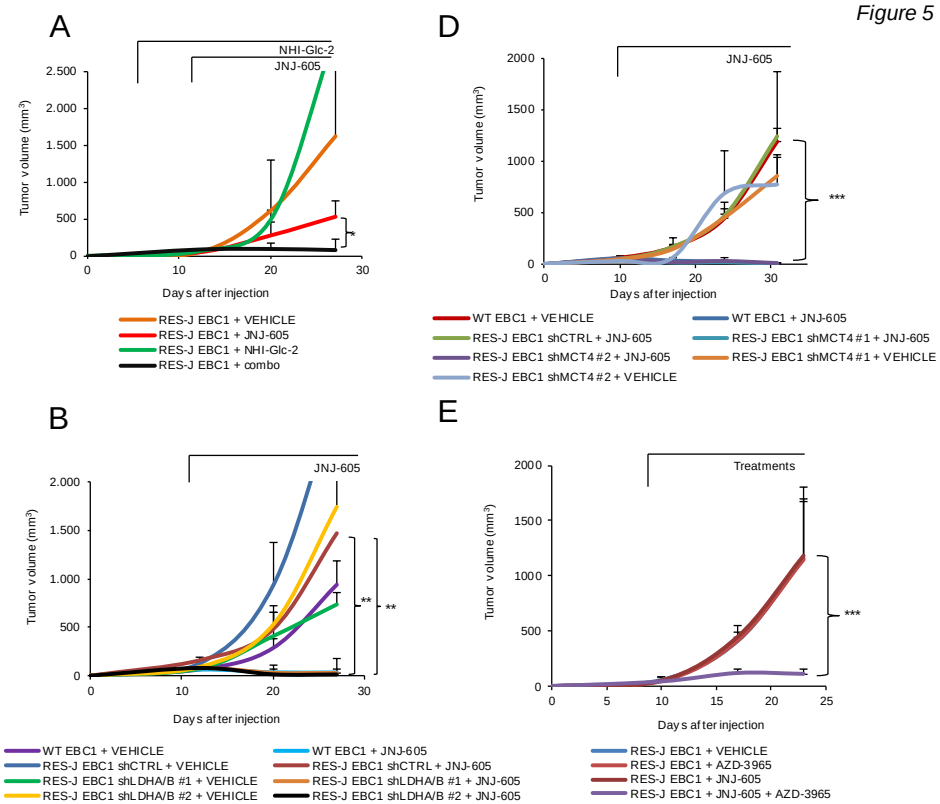
A
NHI-Glc-2
JNJ-605
Tumor volume (mm³)
Days after injection
RES-J EBC1 + VEHICLE
RES-J EBC1 + JNJ-605
RES-J EBC1 + NHI-Glc-2
RES-J EBC1 + combo
D
JNJ-605
***
WT EBC1 + VEHICLE
WT EBC1 + JNJ-605
RES-J EBC1 shCTRL + JNJ-605
RES-J EBC1 shMCT4#1 + JNJ-605
RES-J EBC1 shMCT4#2 + JNJ-605
RES-J EBC1 shMCT4#1 + VEHICLE
RES-J EBC1 shMCT4#2 + VEHICLE
B
JNJ-605
**
**
WT EBC1 + VEHICLE
WT EBC1 + JNJ-605
RES-J EBC1 shCTRL + VEHICLE
RES-J EBC1 shCTRL + JNJ-605
RES-J EBC1 shLDHA/B #1 + VEHICLE
RES-J EBC1 shLDHA/B #1 + JNJ-605
RES-J EBC1 shLDHA/B #2 + VEHICLE
RES-J EBC1 shLDHA/B #2 + JNJ-605
E
Treatments
***
RES-J EBC1 + VEHICLE
RES-J EBC1 + AZD-3965
RES-J EBC1 + JNJ-605
RES-J EBC1 + JNJ-605 + AZD-3965
C
JNJ-605
NHI-Glc-2
Tumor Volume (mm³)
RES-J EBC1 #2
RES-J EBC1 #3
RES-J EBC1 #4
Days after injection

Figure 6

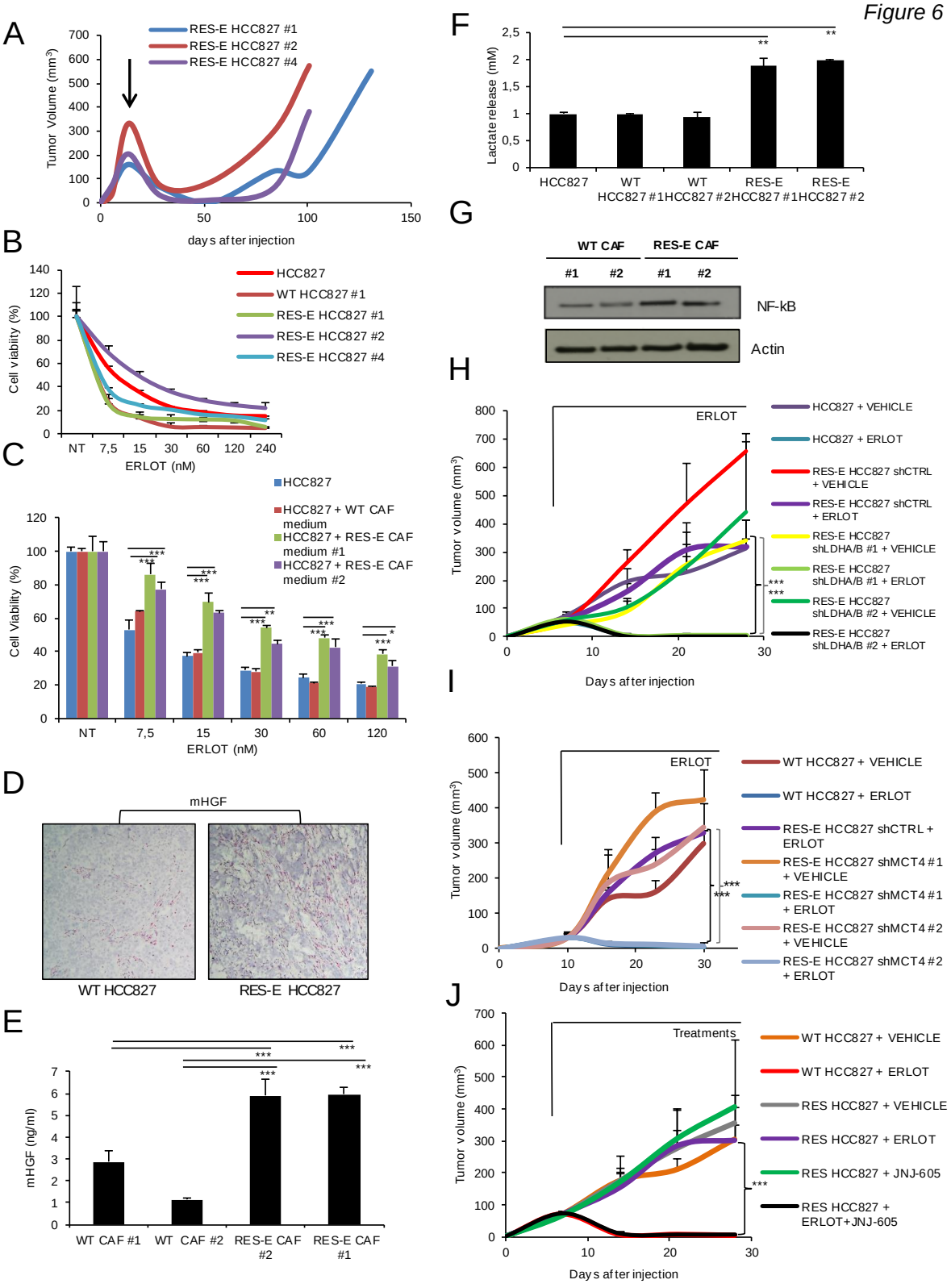
A
RES-E HCC827 #1
RES-E HCC827 #2
RES-E HCC827 #4
Tumor Volume (mm3)
days after injection
B
HCC827
WT HCC827 #1
RES-E HCC827 #1
RES-E HCC827 #2
RES-E HCC827 #4
Cell viability (%)
ERLOT (nM)
C
HCC827
HCC827 + WT CAF medium
HCC827 + RES-E CAF medium #1
HCC827 + RES-E CAF medium #2
Cell Viability (%)
ERLOT (nM)
D
mHGF
WT HCC827
RES-E HCC827
E
mHGF (ng/ml)
WT CAF #1
WT CAF #2
RES-E CAF #2
RES-E CAF #1
F
Lactate release (mM)
HCC827
WT HCC827 #1
WT HCC827 #2
RES-E HCC827 #1
RES-E HCC827 #2
G
WT CAF
RES-E CAF
#1
#2
NF-kB
Actin
H
ERLOT
HCC827 + VEHICLE
HCC827 + ERLOT
RES-E HCC827 shCTRL + VEHICLE
RES-E HCC827 shCTRL + ERLOT
RES-E HCC827 shLDHA/B #1 + VEHICLE
RES-E HCC827 shLDHA/B #1 + ERLOT
RES-E HCC827 shLDHA/B #2 + VEHICLE
RES-E HCC827 shLDHA/B #2 + ERLOT
Tumor volume (mm3)
Days after injection
I
ERLOT
WT HCC827 + VEHICLE
WT HCC827 + ERLOT
RES-E HCC827 shCTRL + ERLOT
RES-E HCC827 shMCT4 #1 + VEHICLE
RES-E HCC827 shMCT4 #1 + ERLOT
RES-E HCC827 shMCT4 #2 + VEHICLE
RES-E HCC827 shMCT4 #2 + ERLOT
Tumor volume (mm3)
Days after injection
J
Treatments
WT HCC827 + VEHICLE
WT HCC827 + ERLOT
RES HCC827 + VEHICLE
RES HCC827 + ERLOT
RES HCC827 + JNJ-605
RES HCC827 + ERLOT+JNJ-605
Tumor volume (mm3)
Days after injection

Figure 7

A

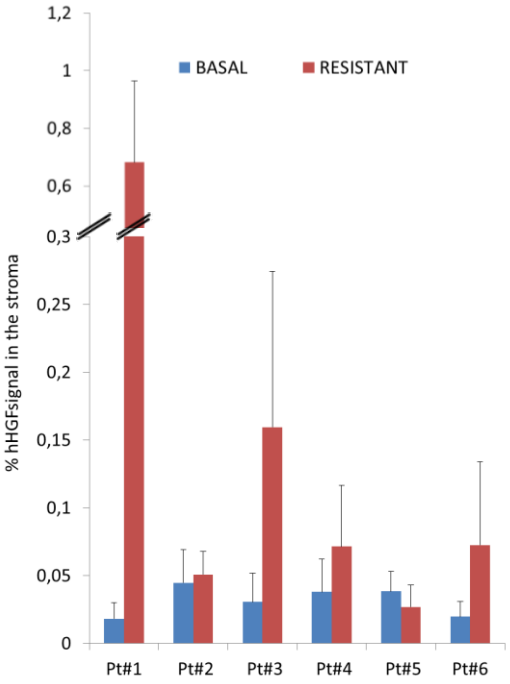

hHGF increase in RESISTANT vs BASAL (FOLDS)	37,7	1,1	5,2	1,9	0,7	3,7

B